

RESEARCH ARTICLE

# Cell-Autonomous and Non-cell-autonomous Function of Hox Genes Specify Segmental Neuroblast Identity in the Gnathal Region of the Embryonic CNS in *Drosophila*

Henrike Becker, Simone Renner, Gerhard M. Technau\*, Christian Berger\*

Institute of Genetics, University of Mainz, Mainz, Germany

\* [bergerc@uni-mainz.de](mailto:bergerc@uni-mainz.de) (CB); [technau@uni-mainz.de](mailto:technau@uni-mainz.de) (GMT)



 OPEN ACCESS

**Citation:** Becker H, Renner S, Technau GM, Berger C (2016) Cell-Autonomous and Non-cell-autonomous Function of Hox Genes Specify Segmental Neuroblast Identity in the Gnathal Region of the Embryonic CNS in *Drosophila*. *PLoS Genet* 12(3): e1005961. doi:10.1371/journal.pgen.1005961

**Editor:** Claude Desplan, New York University, UNITED STATES

**Received:** September 17, 2015

**Accepted:** March 4, 2016

**Published:** March 25, 2016

**Copyright:** © 2016 Becker et al. This is an open access article distributed under the terms of the [Creative Commons Attribution License](https://creativecommons.org/licenses/by/4.0/), which permits unrestricted use, distribution, and reproduction in any medium, provided the original author and source are credited.

**Data Availability Statement:** All relevant data are within the paper and its Supporting Information files.

**Funding:** This work was supported by grants from the Deutsche Forschungsgemeinschaft (DFG, URL: <http://www.dfg.de>) to GMT (TE 130/9-3; GRK 1044-A1). The funders had no role in study design, data collection and analysis, decision to publish, or preparation of the manuscript.

**Competing Interests:** The authors have declared that no competing interests exist.

## Abstract

During central nervous system (CNS) development neural stem cells (Neuroblasts, NBs) have to acquire an identity appropriate to their location. In thoracic and abdominal segments of *Drosophila*, the expression pattern of Bithorax-Complex Hox genes is known to specify the segmental identity of NBs prior to their delamination from the neuroectoderm. Compared to the thoracic, ground state segmental units in the head region are derived to different degrees, and the precise mechanism of segmental specification of NBs in this region is still unclear. We identified and characterized a set of serially homologous NB-lineages in the gnathal segments and used one of them (NB6-4 lineage) as a model to investigate the mechanism conferring segment-specific identities to gnathal NBs. We show that NB6-4 is primarily determined by the cell-autonomous function of the Hox gene *Deformed* (*Dfd*). Interestingly, however, it also requires a non-cell-autonomous function of *labial* and *Antennapedia* that are expressed in adjacent anterior or posterior compartments. We identify the secreted molecule Amalgam (*Ama*) as a downstream target of the Antennapedia-Complex Hox genes *labial*, *Dfd*, *Sex combs reduced* and *Antennapedia*. In conjunction with its receptor Neurotactin (*Nrt*) and the effector kinase Abelson tyrosine kinase (*Abl*), *Ama* is necessary in parallel to the cell-autonomous *Dfd* pathway for the correct specification of the maxillary identity of NB6-4. Both pathways repress *CyclinE* (*CycE*) and loss of function of either of these pathways leads to a partial transformation (40%), whereas simultaneous mutation of both pathways leads to a complete transformation (100%) of NB6-4 segmental identity. Finally, we provide genetic evidences, that the *Ama-Nrt-Abl*-pathway regulates *CycE* expression by altering the function of the Hippo effector Yorkie in embryonic NBs. The disclosure of a non-cell-autonomous influence of Hox genes on neural stem cells provides new insight into the process of segmental patterning in the developing CNS.

## Author Summary

The central nervous system (CNS) needs to be subdivided into functionally specified regions. In the developing CNS of *Drosophila*, each neural stem cell, called neuroblasts (NB), acquires a unique identity according to its anterior-posterior and dorso-ventral position to generate a specific cell lineage. Along the anterior-posterior body axis, Hox genes of the Bithorax-Complex convey segmental identities to NBs in the trunk segments. In the derived gnathal and brain segments, the mechanisms specifying segmental NB identities are largely unknown. We investigated the role of Hox genes of the Antennapedia-Complex in the gnathal CNS. In addition to cell-autonomous Hox gene function, we unexpectedly uncovered a parallel non-cell-autonomous pathway in mediating segmental specification of embryonic NBs in gnathal segments. Both pathways restrict the expression of the cell cycle gene *CyclinE*, ensuring the proper specification of a glial cell lineage. Whereas the Hox gene *Deformed* mediates this cell-autonomously, *labial* and *Antennapedia* influence the identity via transcriptional regulation of the secreted molecule *Amalgam* (and its downstream pathway) in a non-cell-autonomous manner. These findings shed new light on the role of the highly conserved Hox genes during segmental patterning of neural stem cells in the CNS.

## Introduction

The *Drosophila* central nervous system (CNS) consists of 20 segmental units (neuromeres), the sizes and composition of which are specifically adapted to the functional requirements of the respective body parts in the head, thorax and abdomen. Thus, neural stem cells (called neuroblasts, NBs), although showing serial homologies among segments, generate distinct cell lineages in correspondence to their segmental assignment [1]. This segmental identity is conferred to NBs already in the embryonic neuroectoderm and persists during the generation of their larval and adult sublineages. Therefore, it is convenient to study mechanisms regulating the segmental specification of neural stem cells in the embryo.

Most studies on segmental specification of embryonic NBs in *Drosophila* were focused so far on thoracic (T1-T3) and abdominal (A1-A10) segments of the ventral nerve cord (VNC). Neuromeres T1-A7 are built by a stereotype pattern of approximately 30 NBs per hemisegment. Individual identities and serial homology of segmentally repeated NBs is reflected by position, marker gene expression [2, 3] and composition of their lineages [4–6]. However, some of the serially homologous NB-lineages exhibit specific differences between thoracic and abdominal segments, which are conveyed to NBs already in the neuroectoderm by Bithorax-Complex (Bx-C) Hox genes [7–9]. While thoracic identities seem to represent a ground state (T2, no input of Hox genes; [10]), identities of consecutive posterior segments are established by adding the function of Bx-C Hox genes *Ultrabithorax* (*Ubx*), *abdominal-A* (*abdA*) and *Abdominal-B* (*AbdB*), an evolutionary highly conserved phenomenon described as posterior dominance or prevalence of Hox genes [10–12]. The terminal abdominal neuromeres A8-A10 exhibit a progressively derived character regarding size and composition. In these segments, NB patterns and segmental identities are controlled by combined action of the Hox gene *AbdB* and the ParaHox gene *caudal* [13, 14].

The *Drosophila* head consists of seven segments (4 pregnathal and 3 gnathal) all of which contribute neuromeres to the CNS [15, 16]. The brain is formed by approximately 100 NBs per hemisphere, which have been individually identified and assigned to specific pregnathal segments [17, 18]. As judged from comparison of the combinatorial codes of marker gene

expression only few brain NBs appear to be serially homologous to NBs in the thoracic/abdominal ventral nerve cord, reflecting the highly derived character of the brain neuromeres [19]. The connecting tissue between brain and the thoracic VNC consists of three neuromeres formed by the gnathal head segments named mandibular (mad), maxillary (max) and labial (lab) segment, but the number and identity of the neural stem cells and their lineage composition in these segments is still unknown. Compared to the thoracic ground state the segmental sets of gnathal NBs might be reduced to different degrees, but are thought to be less derived compared to the brain NBs. Therefore, to fully understand segmental specification during central nervous system development, it is important to identify the neuroblasts and their lineages in these interconnecting segments.

Assuming that most NBs in the gnathal segments still share similarities to thoracic and abdominal NBs, we searched in these segments for serially homologous NB-lineages, which are suitable for genetic analyses. Using the molecular marker *eagle* (*eg*), which specifically labels four NB-lineages in thoracic/abdominal hemisegments [20, 21] we identified three serial homologs (NB3-3, NB6-4 and NB7-3) in the gnathal region. To investigate the mechanisms conferring segmental identities, we focused on one of them, the NB6-4 lineage, which shows the most significant segment-specific modifications. Our analysis reveals a primary role of the Antennapedia-Complex (Antp-C) Hox gene *Deformed* (*Dfd*) in cell-autonomously specifying the maxillary fate of NB6-4 (NB6-4max). Surprisingly, we uncovered an additional, non-cell-autonomous function of the Antp-C Hox genes *labial* (*lab*, expressed anterior to *Dfd*) and *Antennapedia* (*Antp*, expressed posterior to *Dfd*) in specifying NB6-4max. In a mini-screen for downstream effectors we identify the secreted protein Amalgam (*Ama*) to be positively regulated by *lab*, *Dfd* and *Antp* and negatively regulated by the Antp-C Hox gene *Sex combs reduced* (*Scr*). Loss of function of *Ama* and its receptor *Neurotactin* (*Nrt*) [22–25] as well as the downstream effector kinase *Abelson tyrosine kinase* (*Abl*) [23] lead to a transformation of NB6-4max similar to *Dfd* single mutants. Thus, in parallel to the cell-autonomous role of *Dfd*, a non-cell-autonomous function of Hox genes *lab* and *Antp*, mediated via the *Ama-Nrt-Abl* pathway, is necessary to specify NB6-4max identity. Disruption of either of these pathways leads to a partial misspecification of NB6-4max (approx. 40%), whereas simultaneous disruption of both pathways leads to a complete transformation (approx. 100%) of NB6-4max to a labial/thoracic identity. We further show that both pathways regulate the expression of the cell cycle gene *CyclinE*, which is necessary and sufficient to generate labial/thoracic NB6-4 identity. Whereas *Dfd* seems to directly repress *CyclinE* transcription (similar to *AbdA/AbdB* in the trunk) [26], we provide indications that the *Ama-Nrt-Abl* pathway prevents *CyclinE* expression by altering the activity of the Hippo/Salvador/Warts pathway effector Yorkie (*Yki*).

## Results

### Identification of serially homologous Eagle-positive NB-lineages and variations of the Eagle-pattern in gnathal segments

To identify serially homologous NBs in the gnathal segments, we used the transcription factor Eagle (*Eg*) as a marker. In the well-studied thoracic and abdominal segments *Eg* is expressed in four NBs and their lineages: NBs 2–4, 3–3, 6–4 and 7–3 [20, 21]. Staining WT embryos at stage11 (st11) with *Eg* and the NB-marker *Deadpan* (*Dpn*) (Fig 1A) [27] reveals a reduced number of *Eg*-positive NBs in gnathal segments. Using *Eg* and *Dpn* to identify NB2-4 [28] we observed, that NB2-4 is missing in all three gnathal segments (Fig 1). Co-staining of *Eg* and *Runt* at st12 identifies NB3-3 [29] in labial and maxillary segments, but not in the mandibular segment (Fig 1B). *Eg* and *Engrailed* (*En*) co-expression and its position in a typical dorso-posterior area of the *En* stripe indicates the presence of NB7-3 [20, 30] in all three gnathal

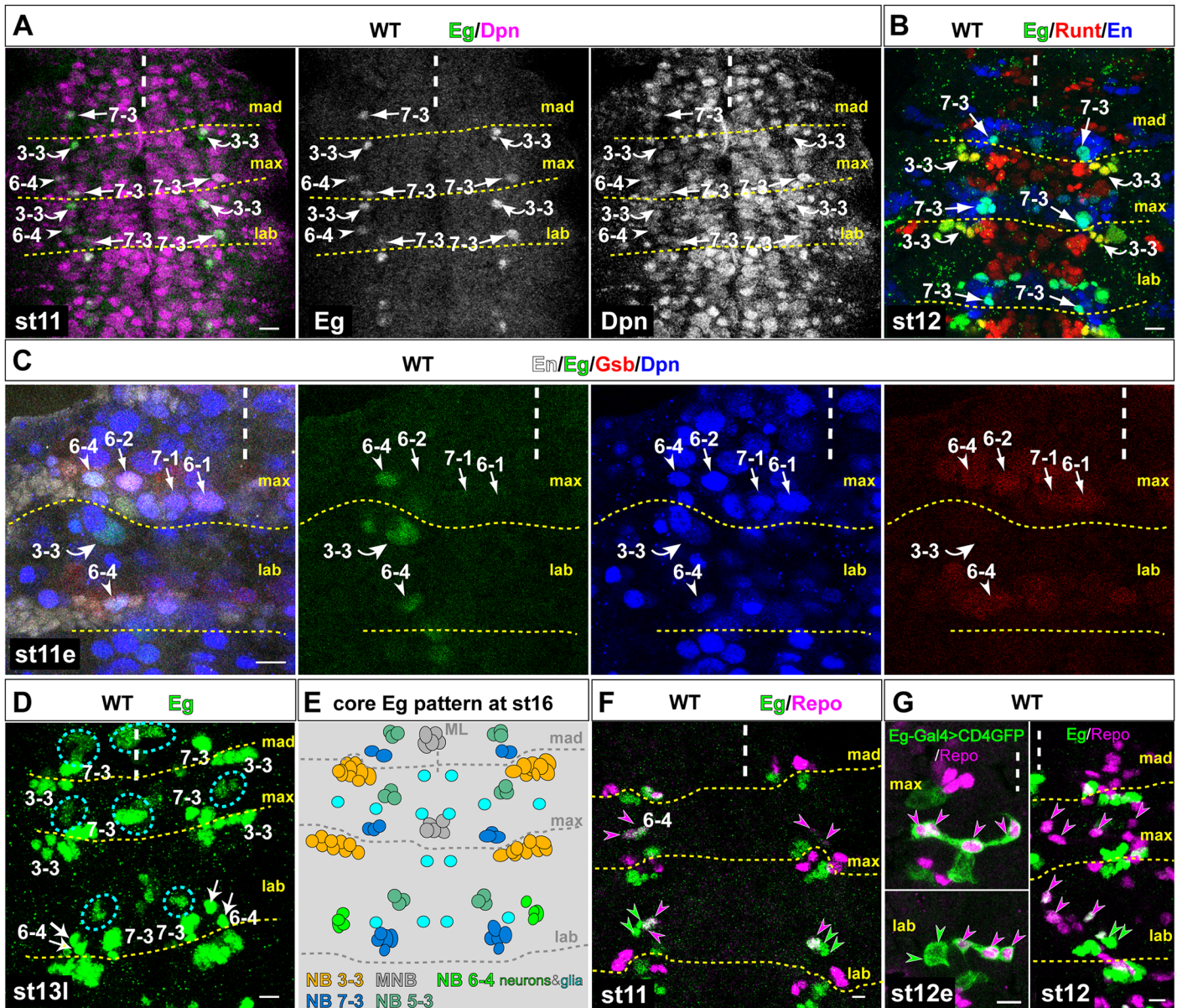


**Fig 1. Description of the Eagle-positive Neuroblast-lineages in embryonic gnathal segments.** (A) Identification of Eagle (Eg) expressing neuroblasts (NBs) in filet preparations of wild type gnathal CNS segments at embryonic stage 11. NBs were stained with Deadpan (Dpn) antibody (magenta); NBs 3–3, 6–4 and 7–3 were identified by co-staining with Eg antibody (green). Middle panel shows Eg channel in monochrome, right panel shows Dpn channel in monochrome. (B) NB3–3 can be identified by co-staining of Eg and Runt antibody (red), NB7–3 can be identified by co-staining of Eg and the segmental marker En (blue) and its typical dorso-medial position. (C) Co-staining of Eg (green), En (white), Dpn (blue) and Gooseberry (Gsb, red) antibody identifies NB6–4 and the presence of Gsb-positive/Eg-negative NB6–2, NB7–1 and NB6–1. (D) Additional cells (cyan circles) express Eg from stage 13 onwards. Progeny of MNB can be identified in the midline of mad and max segments and progeny of NB5–3 can be identified in all three segments. For identification of these cells see [S1 Fig](#) (E) Schematics of the core Eg expression pattern at stage 16. For simplicity extra Eg-positive cells are not highlighted. For complete pattern see [S1](#) and [S2 Figs](#). (F) Co-staining of Eg (green) with Repo (magenta) antibody reveals a pure glial NB6–4 lineage in maxillary segment and a mixed neuronal/glial lineage in the labial segment. (G) At stage 12 the maxillary NB6–4 lineage consists of four glial cells (magenta arrow heads), two medial and two lateral cell-body glial cells. The labial NB6–4 generates a dorso-lateral cluster of 4–5 neurons (green arrow heads) and three cell-body glial cells (magenta arrow heads) of which one is located ventro-laterally and two are in a ventro-medial position. The left panels shows *egGal4* expressing *UAS-CD4::gfp* to show the clonal relation and to identify the four glial cells in the maxillary segment. In this and all following figures if not stated differently: anterior is up, dashed white line represents the midline, dashed yellow lines indicate segmental boundaries, mad, mandibular segment, max, maxillary segment and lab, labial segment, numbers indicate NBs or NB-lineages (e.g. 7–3 indicates NB7-3), magenta arrow heads indicate NB6–4 glioblast or its glial progeny cells, green arrow heads indicate NB6–4 neuronal daughter precursor or neuronal progeny cells, WT, wild type, st, stage, l, late, e, early, m, middle. Scale bar is 10  $\mu$ m.

doi:10.1371/journal.pgen.1005961.g001

segments (Fig 1A and 1B). NB6-4 is identifiable by combined expression of Eg, En and Gooseberry (Gsb)[31, 32] in labial and maxillary segments but is missing in the mandibular segment (Fig 1A and 1C).

Next we used Eg in combination with various other markers at st13 to st16 to describe the composition of the Eg-positive lineages (Figs 1D, 1E and S1). NB3-3 generates a lineage of approximately 9 neurons, which is less than described for thoracic/abdominal lineages with 10–13 cells [6]. Among these we observed 7 neurons expressing Even-skipped (Eve) in maxillary and labial segments (S1A Fig), compared to 5 (on average) in the thoracic and 9 (on average) in the abdominal lineages [6, 14, 33].

The early NB7-3 lineage consist of six to seven cells, expressing the marker Eyeless (Ey; Figs 1E and S1B) [13, 34]), but due to segment-specific cell death at later stages [35, 36] the cell numbers in each segment are distinct. At st16 we find the mandibular NB7-3mad lineage to consist of two cells, the maxillary NB7-3max of three cells and the labial NB7-3lab of three to five cells (Fig 1E). In comparison, in T1 and T2 the late embryonic NB7-3 lineage consists of four, in T3-A7 of three, in A8 of two or three, and in A9 and A10 NB7-3 is not formed [14, 36].

NB6-4 generates a mixed neuronal/glial lineage (4–5 neurons, 3 glia) in labial segments as revealed by staining against Eg and the glial marker Repo (Fig 1E–1G)[37]. Its division pattern is identical to thoracic NB6-4, in which the first division separates a glial from a neuronal daughter precursor and factors like Prospero or *glia cells missing* (*gcm*) (S1C Fig) are asymmetrically localized to the glial progenitor [7, 38–40]. In contrast, similar to NB6-4 in abdominal segments [6], NB6-4max is a pure glioblast, generating four glial progeny cells (Fig 1E–1G).

To our surprise, we observed more Eg-positive cell clusters in gnathal segments from st12 onwards (Figs 1D, 1E, S1 and S2), that we could identify as progeny of the Midline Neuroblast (MNB, in mad and max segments), progeny of the NB5-3 (in all three segments) [41–45] and from stage 14 onwards we could identify Eg-positive late progeny of NBs 6–2, 4–3, 4–4 and 5–6 (in mad and max segments). Further details can be found in Figs 1D, 1E, S1 and S2.

Taken together, we show that (1) despite of its complex expression pattern in the late embryo, Eg is a reliable marker to identify serially homologous NBs and their progeny in gnathal segments, (2) whereas NB2-4 is missing in all gnathal segments, NB3-3 and NB6-4 are present in labial and maxillary segments, and NB7-3 is present in all three gnathal segments, (3) segment-specific differences occur in the NB7-3 lineage with regard to neuronal cell numbers, and in the NB6-4 lineage with regard to cell types: While NB6-4lab gives rise to a mixed neuronal/glial lineage corresponding to the thoracic homologs, NB6-4max is a pure glioblast corresponding to the abdominal homologs.

In the following we will focus on the NB6-4 lineage to elucidate the mechanism conferring segmental specificities in the gnathal CNS.

### ***Deformed* and *Sex combs reduced* are co-expressed in NB6-4max, and NB6-4lab expresses *Antennapedia***

Since it was shown for thoracic/abdominal segments that Bx-C Hox genes convey the regional specification on the progenitor level [9, 13, 46], we next analyzed the mRNA expression pattern of Antp-C genes *labial* (*lab*), *Deformed* (*Dfd*), *Sex combs reduced* (*Scr*) and *Antennapedia* (*Antp*) in the presumptive neuroectoderm of maxillary and labial segments from st4 onwards. The widths of the mRNA stripes were measured in whole mount embryos using the distance from the anterior pole in relation to the length of the whole egg (EL; see [material and methods](#); S3 Fig). Fig 2A shows the average expression domains in st6, st7 and st8 schematically. In contrast to earlier reports [47, 48], we could detect an overlap of *Dfd* and *Scr*-mRNA expression from st6 onwards (due to tissue invagination in the cephalic furrow at st7 this overlap is hardly

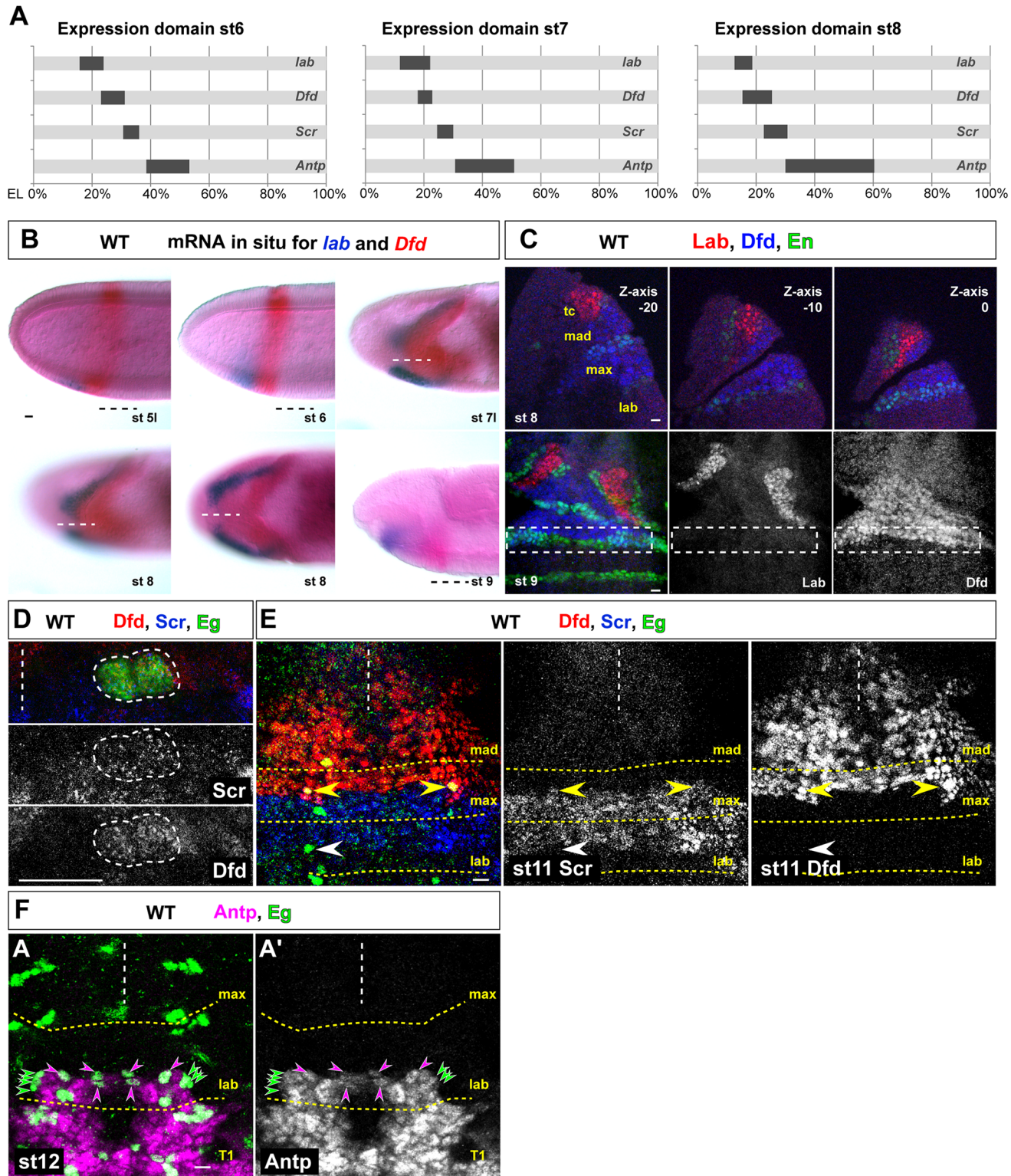


**Fig 2. Expression pattern of Hox genes in embryonic gnathal segments.** (A) Schematic representation of the average mRNA expression domains (in % of whole egg length, EL) of the Hox genes *labial* (*lab*), *Deformed* (*Dfd*), *Sex combs reduced* (*Scr*) and *Antennapedia* (*Antp*) at stage 6, 7 and 8. For original staining see S3 Fig. (B) Double *in-situ* hybridization to visualize expression pattern of *lab* (blue) and *Dfd*-mRNAs (red) at stage 5I to 9. No co-expression can be observed. Anterior to the left. Dashed line marks the ventral midline. (C) Antibody staining in the maxillary segment to visualize the protein expression pattern of Lab (red) and Dfd (blue) in relation to the Engrailed (En, green) domain from which NB6-4 segregates. No co-expression can be observed in stage

8 or 9. Upper panel shows three successive focal planes of a lateral view (anterior up, ventral to the right) of a whole mount embryo (Z-axis from -20, -10 to 0  $\mu\text{m}$ ). Tc, tritocerebrum. Lower panel shows filet preparation (anterior up, ventral view). The dash-lined box indicate the En-positive domain, from which NB6-4 delaminates; no expression of Lab can be observed. (D) Dfd (red) and Scr (blue) are co-expressed in the maxillary NB6-4 (Eg, green); two-cell stage shown at late stage 11. (E) NB6-4 expresses Dfd (red) and Scr (blue) in the maxillary segment (yellow arrow head), whereas NB6-4 in the labial segment lacks both of them (white arrow head). (F) All cells of the NB6-4 lineage in the labial segment express Antp (magenta). T1, first thoracic segment. Scale bar is 10  $\mu\text{m}$ .

doi:10.1371/journal.pgen.1005961.g002

visible, compare to Fig 2B) in the presumptive neuroectoderm of NB6-4max. The presumptive neuroectoderm of NB6-4lab shows *Antp*-mRNA expression only. In st7/8 it seemed that *lab*-mRNA expression was overlapping with *Dfd*-mRNA (Fig 2A), but close investigation showed, that due to the morphogenetic movements during cephalic furrow formation two epithelial sheets are overlapping but no co-staining can be found in cells of the neuroectoderm from which NB6-4max will delaminate (Fig 2B). We confirmed our observations using antibody staining against Lab, Dfd and the segmental marker En and could not observe a co-staining of Lab and Dfd in the maxillary stripe at st8/9, which is prior to NB6-4 delamination from the neuroectoderm (Fig 2C, see also [49]). Next we performed antibody staining for Dfd, Scr and Antp together with Eg and could indeed verify that NB6-4max co-expresses Dfd and Scr (Fig 2D and 2E), whereas NB6-4lab expresses Antp (Fig 2F) and no Scr. We also tested for Proboscipedia (Pb) expression and could observe single cell clusters distributed over the whole CNS [47] but we could not detect Pb expression in NB6-4 in gnathal segments (S4O Fig).

Therefore, of all Antp-C genes tested on mRNA and protein level, Dfd and Scr are expressed in NB6-4max, whereas NB6-4lab expresses Antp. *labial* and *Antp* are neither expressed in the maxillary neuroectoderm nor in the neuroblast NB6-4max itself.

### Segment specificity of NB6-4max is primarily determined by *Deformed*, but influenced in a parallel mechanism by *labial* and *Antennapedia*

To analyze the influence of Hox genes on the segmental identity of NB6-4 in gnathal segments, we next tested different single or double mutants and overexpression of Antp-C genes (Fig 3A shows wild type). We first analyzed *Antp* loss-of-function (LoF) alleles *Antp*<sup>25</sup> and *Antp*<sup>11</sup> and could not observe a change in the segmental identity of both NB6-4max and NB6-4lab (*Antp*<sup>25</sup>, n = 50 maxillary hemisegments (mHs); *Antp*<sup>11</sup>, n = 50 mHs; Fig 3B shows *Antp*<sup>25</sup>; since different mutant Hox gene alleles revealed similar phenotypes we show in this and the following experiments the results for only one allele). Furthermore, overexpression of *Antp* has no effect on the NB6-4 lineage identity in any segment (n = 50 mHs; Fig 3C). Therefore, similar to the thoracic NB6-4 lineages [46] the labial NB6-4 identity represents a ground state, which does not require Hox gene function.

Next, we tested the LoF alleles *Dfd*<sup>16</sup>, *Dfd*<sup>12</sup> and *Dfd*<sup>11</sup> for their impact on NB6-4max. Double staining against Eg and the glial cell marker Repo revealed that loss of *Dfd* leads to a homeotic transformation of NB6-4max into a mixed lineage comprising neurons and glial cells (corresponding to NB6-4lab lineage) in approximately 43% of all hemisegments (*Dfd*<sup>16</sup> n = 650 mHs, *Dfd*<sup>12</sup> n = 650 mHs; *Dfd*<sup>11</sup> n = 650 mHs; Fig 3D shows *Dfd*<sup>16</sup>). Since NB6-4max expresses Dfd and Scr, we analyzed two LoF alleles of *Scr* (*Scr*<sup>17</sup> (n = 500 mHs) and *Scr*<sup>11</sup> (n = 500 mHs)). In 10% of the mutant hemisegments NB6-4max produces neurons and glial cells (Fig 3E shows *Scr*<sup>17</sup>). As this suggests that *Dfd* and *Scr* might act synergistically, we analyzed the effect of double LoF of *Dfd*<sup>16</sup> and *Scr*<sup>4</sup> (n = 500 mHs). Surprisingly, instead of an increase in the transformation rate we could observe a reduced transformation rate in NB6-4max (17%; Fig 3F) compared to single *Dfd* LoF situation (Fig 3D, 43%). In addition, whereas ectopic expression of *Scr* (n = 50 mHs) has no effect on labial (S4A Fig) and thoracic NB6-4 (Fig 3G), the ectopic expression of *Dfd* leads to a transformation of labial (S4B Fig) and

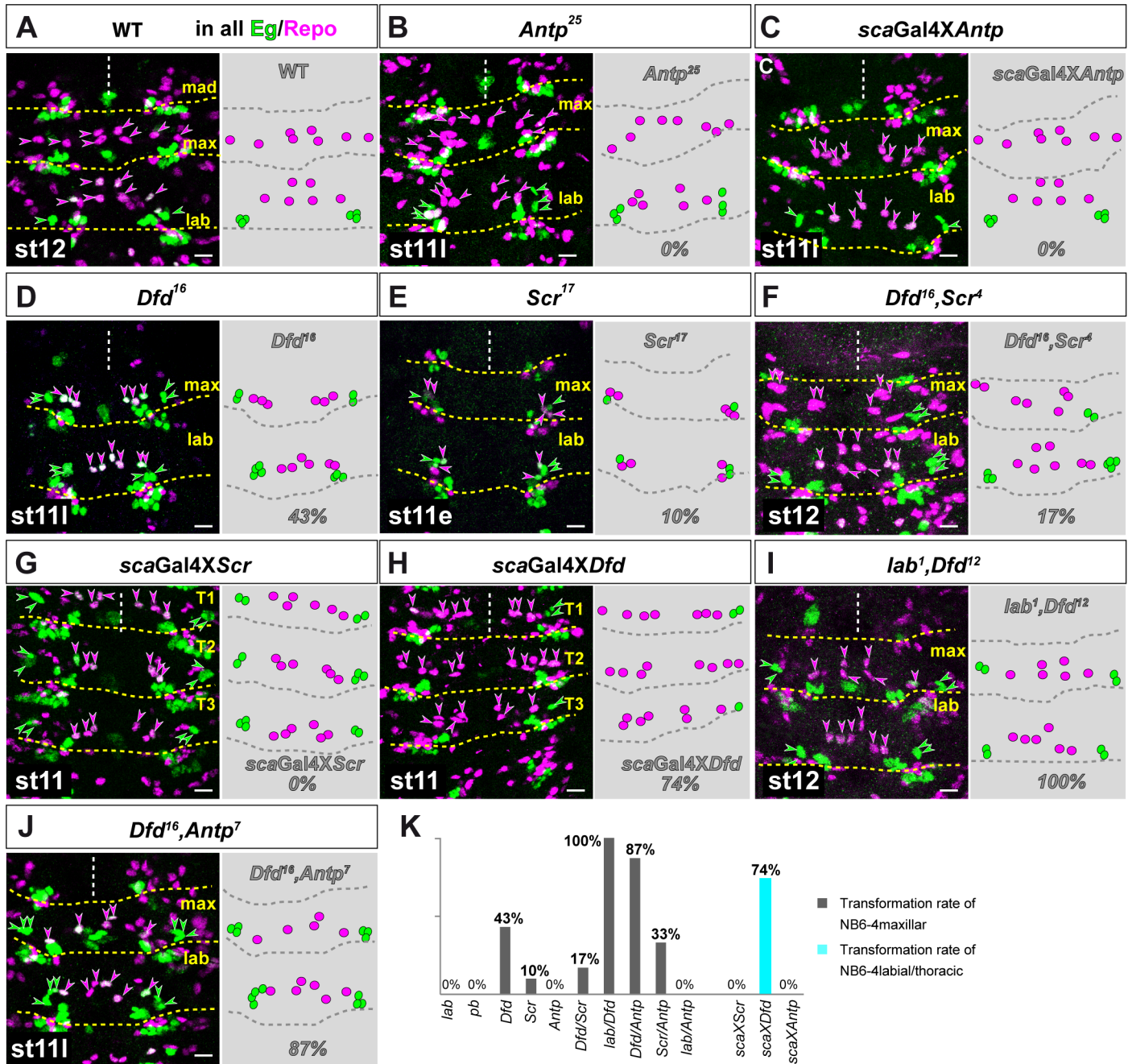


**Fig 3. Segment specificity of NB6-4max is primarily determined by *Deformed*, but influenced in a parallel mechanism by *labial* and *Antennapedia*.** For all images (A-J): Magenta arrow heads or spheres depict NB6-4-derived glial cells, green arrow heads or spheres depict NB6-4-derived neuronal cells. Segments are indicated. Right side shows an illustration of the composition of the NB6-4 lineage in the respective segments. Percentage gives transformation rate of NB6-4. (A) Wild type lineages of NB6-4 in maxillary and labial segments. NB6-4 generates 4 glial cells per maxillary hemisegment and 3 glial cells and a neuronal cluster per labial hemisegment. (B) In *Antennapedia* (*Antp*<sup>25</sup>) mutants NB6-4 cell fate is not altered in maxillary or labial segments. (C) Ectopic expression of *Antp* using the *scabrous*-Gal4 (*scaGal4*) line does not alter NB6-4 cell fates in maxillary or labial segments. (D) Mutation in *Deformed* (*Dfd*<sup>16</sup>) leads to a transformation of NB6-4max glioblast into a neuroglioblast in 43% of all hemisegments. (E) Mutation in *Sex combs reduced* (*Scr*<sup>17</sup>) leads to a transformation of NB6-4max glioblast into a neuroglioblast in 10% of all hemisegments. (F) Double mutation of *Dfd*<sup>16</sup> and *Scr*<sup>4</sup> leads to a reduction of the transformation rate (17%) compared to *Dfd* single mutants (Fig 3D, 43%). *Dfd* and *Scr* do not act synergistically. (G) Ectopic expression of *Scr* using the *scabrous*-Gal4 (*scaGal4*) line does not alter NB6-4 cell fates in thoracic or labial (see S4A Fig) segments. (H) Ectopic expression of *Dfd* using the *scabrous*-Gal4 (*scaGal4*) line transforms thoracic and labial (see S4B Fig) NB6-4 into a maxillary fate producing only glial cells in 74% of all thoracic hemisegments. (I) Double mutation of *lab*<sup>1</sup> and *Dfd*<sup>12</sup> leads to a complete transformation of NB6-4max glioblast fate into a labial/thoracic neuroglioblast fate in 100% of all hemisegments. (J) Double mutation of *Dfd*<sup>16</sup> and *Antp*<sup>7</sup> leads to a nearly complete transformation of NB6-4max glioblast fate into a labial/thoracic



neuroglioblast fate in 87% of all hemisegments. (K) Summary diagram of transformation rates in NB6-4maxillary (grey bars) or NB6-4labial/thoracic (cyan bars) in the respective mutant or ectopic expression situation. Transformation rates are given in percentage of analyzed hemisegments (number of hemisegments see text). Scale bar is 10  $\mu$ m.

doi:10.1371/journal.pgen.1005961.g003

thoracic NB6-4 (74% of all hemisegments ( $n = 160$  mHs), Fig 3H) towards a maxillary identity with four glial cells and no neurons. Thus, *Dfd* seems to be the major Hox gene influencing the NB6-4max identity cell-autonomously. Since loss of function only leads to a partial transformation rate (43%), we wondered if any of the other Antp-C genes, although not expressed in NB6-4, might be involved in specifying NB6-4max. Surprisingly, we observed an increase of the transformation rate in double LoF of *lab*<sup>1</sup>/*Dfd*<sup>12</sup> (100%,  $n = 650$  mHs, Fig 3I) and *Dfd*<sup>16</sup>/*Antp*<sup>7</sup> (87%,  $n = 650$  mHs, Fig 3J) compared to 43% in single *Dfd* mutants (Fig 3D). None of the single mutant alleles of *lab*<sup>4</sup> ( $n = 50$  mHs, S4C Fig) or *Antp*<sup>25</sup> (see above) or the double LoF of *lab*<sup>1</sup> and *Antp*<sup>25</sup> ( $n = 100$  mHs, S4D Fig) showed any change of the identity of NB6-4max. To show that loss of Hox gene function leads to a transformation of the maxillary NB6-4 on the progenitor level, we stained *lab*<sup>1</sup>/*Dfd*<sup>12</sup> mutants for Eg and *gcm*-mRNA. Whereas the wild type NB6-4max distributes *gcm*-mRNA equally to both daughter cells (see S1C Fig), the transformed NB6-4 in maxillary segments of *lab*<sup>1</sup>/*Dfd*<sup>12</sup> mutants shows an asymmetrically distribution of *gcm*-mRNA to the glial sublineage only (S4E Fig), like wild type labial (see S1C Fig) or thoracic [7, 38–40] progenitors do. Furthermore, the loss of *Scr* together with *Antp* increased the transformation rate to 33% ( $n = 100$  mHs; S4F Fig) compared to 10% for *Scr* LoF alone.

Since neither *Antp* nor *lab* is expressed in wild type NB6-4max, we next investigated if the expression pattern of Hox genes is altered in mutant background. In *Dfd* mutants we could not detect any changes in Hox gene expression (single or double mutants, S4G–S4N Fig) with the exception of a slight extension of the *lab* expression domain towards the anterior mandibular segment (see also [50]) and a loss of Scr protein in NB6-4max. This protein loss seems to be due to a translational repression of Scr, since we detected normal expression of *Scr*-mRNA in *Dfd* mutants (S4H Fig).

Taken together, our expression and mutant analyses reveals a cell-autonomous function of *Dfd* and *Scr* in specifying NB6-4max (Fig 3K). *Dfd* seems to be the major cell-autonomously acting Hox gene in NB6-4max, since only ectopic expression of *Dfd*, but not *Scr*, can transform NB6-4lab/thoracic into a maxillary identity. Surprisingly, we detected a non-cell-autonomous effect of the more anterior expressed *lab* and the more posterior expressed *Antp* gene. Since these two genes are normally not expressed in NB6-4max nor in the neuroectodermal primordium and we did not observe mis-regulation of other Hox genes in NB6-4max in any Antp-C-mutant situation, we conclude that Lab and Antp act in a non-cell-autonomous manner to contribute to the determination of the maxillary segmental specificity of NB6-4.

To identify potential effectors downstream of the non-cell-autonomously acting Hox genes *lab* and *Antp* in NB6-4max specification, we next conducted a mini-screen.

### A mini-screen for novel regulators of NB6-4max specification identifies the secreted protein Amalgam as potential Hox gene target

Since we uncovered a non-cell-autonomous function of *lab* and *Antp* in specifying the segmental fate of NB6-4max, we performed a mini-screen to identify candidate genes (Fig 4A) affected by and downstream of Hox genes. Candidate genes were selected based on existing studies on Hox downstream targets [51, 52] as well as previously identified potential modifiers of Hox genes [53–57]. We also analyzed a number of non-homeotic genes that are located in the Antp-gene cluster on chromosome 3R. Considering that Hox genes convey a non-cell-

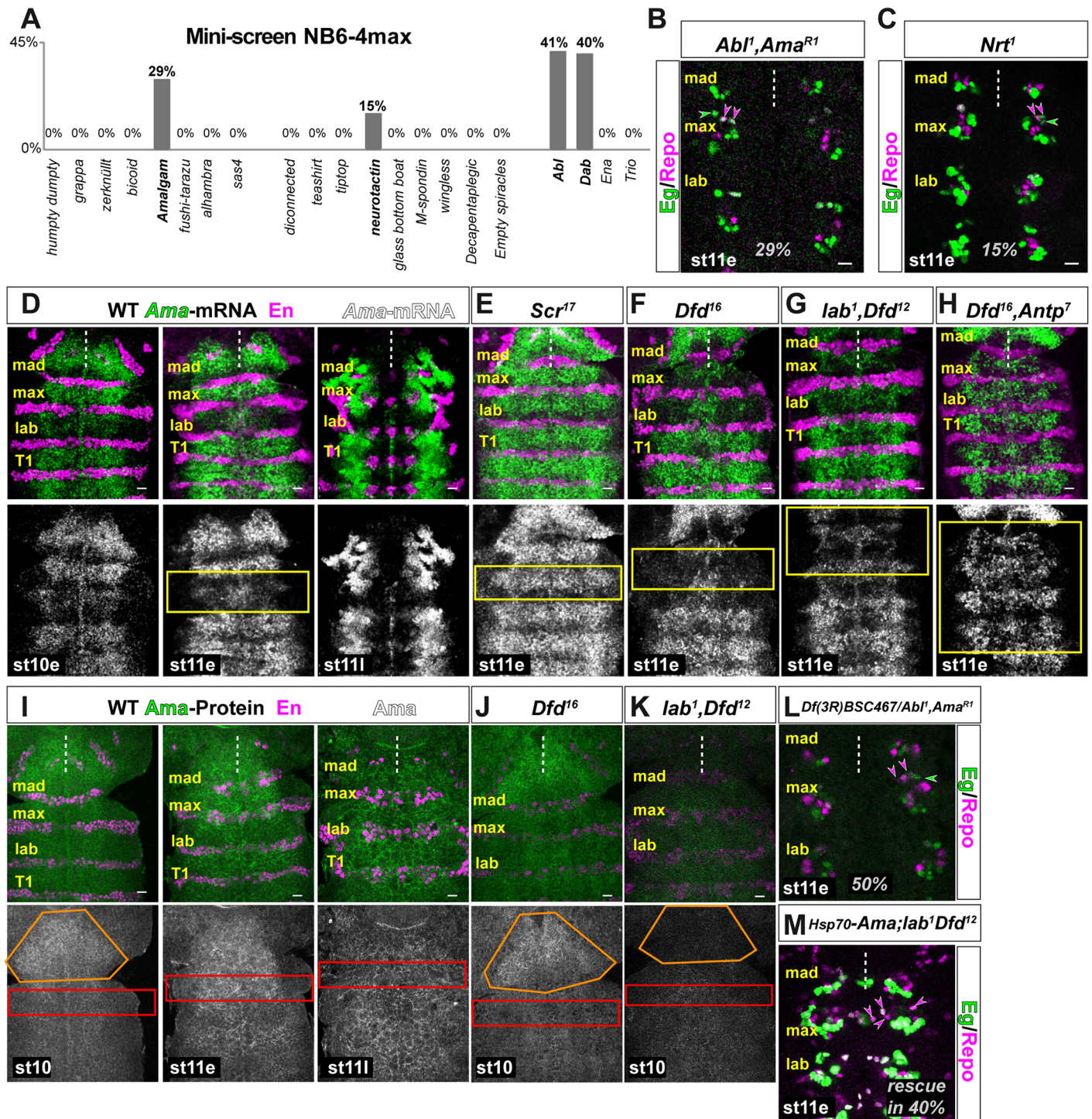


**Fig 4. A mini-screen for novel regulators of NB6-4max specification identifies the secreted protein Amalgam as potential Hox target.** (A) Mutant mini-screen for potential Hox target genes influencing NB6-4max segmental specification. Transformation rates of NB6-4max are given in percentage of analyzed maxillary hemisegments (number of hemisegments see text). (B) Double mutation of *Abi<sup>1</sup>* and *Ama<sup>R1</sup>* leads to a transformation of NB6-4max into a neuroglioblast in 29% of all hemisegments. (C) Mutation of *Nrt<sup>1</sup>* leads to a transformation of NB6-4max into a neuroglioblast in 15% of all hemisegments. (D) Distribution of *Ama* mRNA (in green) in the neuroectoderm/nervous system of gnathal segments at early stage 10 (left panel), early stage 11 (middle panel) and late stage 11 (right panel) by *in situ* hybridization; lower panel displays corresponding channel in monochrome. The segmental marker Engrailed (*En*) is shown in magenta. Yellow box indicates parasegment 2 that is determined by *Scr* and shows reduced expression of *Ama* mRNA. (E-H) *Ama* mRNA expression (green; lower panel monochrome) in mutant backgrounds; compare to wild type expression shown in the middle panel of (D) at early stage 11. (E) *Scr<sup>17</sup>* mutation shows up-regulation of *Ama* mRNA expression in parasegment 2 indicated by the yellow box. (F) *Dfd<sup>16</sup>* mutation shows down-regulation of

*Ama* mRNA expression in posterior mandibular and maxillary regions (yellow box). (G) Double mutation for *lab*<sup>1</sup> and *Dfd*<sup>12</sup> shows down-regulation of *Ama* mRNA expression in mandibular and maxillary regions (yellow box). (H) Double mutation for *Dfd*<sup>16</sup> and *Antp*<sup>7</sup> shows down-regulation of *Ama* mRNA expression in the region of mandibular to thoracic segments (yellow box). (I) Distribution of *Ama* protein (in green) in the neuroectoderm/nervous system of gnathal segments at stage 10 (left panel), early stage 11 (middle panel) and late stage 11 (right panel) by antibody staining. Lower panel shows corresponding *Ama* channel in monochrome. In magenta is the segmental marker En. Red box indicates the region of NB6-4max. Orange box indicates the distribution of *Ama* in mandibular and more anterior regions. (J, K) Compare the *Ama* expression patterns to the wild type expression shown in the middle panel of (I) at stage 10. (J) *Dfd*<sup>16</sup> mutation shows no significant change of *Ama* protein distribution in the region of NB6-4max (red box) presumably due to secreted *Ama* invading from anterior (orange box) and posterior source. (K) Double mutation for *lab*<sup>1</sup> and *Dfd*<sup>12</sup> shows reduced *Ama* distribution in the region of NB6-4max and significant reduction of *Ama* in more anterior regions (orange box). (L) Transheterozygous mutation for the deficiency *Df(3R)BSC467* covering *Dfd* and *Ama* and *Abl*<sup>1</sup>, *Ama*<sup>F1</sup> shows an increase in the transformation rate to 50% in NB6-4max suggesting a synergistic effect of the *Dfd*- and the *Ama*-pathway. (M) Heatshock-induced expression of *Ama* in the *lab*<sup>1</sup>/*Dfd*<sup>12</sup> double mutant rescues the transformation phenotype of NB6-4max in 40% of all hemisegments leading to an overall transformation of 60% (*lab*<sup>1</sup>/*Dfd*<sup>12</sup> show 100% transformation). Scale bar is 10 μm.

doi:10.1371/journal.pgen.1005961.g004

autonomous function we speculated that genes involved in signaling pathways, secreted molecules or genes known to interact with secreted molecules might be promising candidates.

These criteria supplied us with 17 candidate genes, and we tested their LoF with *Eg/Repo* double labeling for defects in the specification of NB6-4max identity. Whereas most of the candidates did not show any abnormal phenotype of the NB6-4 lineage (Fig 4A), the LoF of two of these genes resulted in a transformation of NB6-4max to NB6-4lab/thoracic identity: the secreted adhesion molecule *Amalgam* (Fig 4B, 29%, n = 160 mHs), and its potential receptor *Neurotactin* (*Nrt*, Fig 4C, 15%, n = 120 mHs)[22–25]. *Amalgam* (*Ama*) is located in the *Antp-C* on chromosome 3R [24]. All available *Ama* mutant stocks are combined with the mutant allele of the *Abl* tyrosine kinase *Abl*<sup>1</sup> (*Abl*<sup>1</sup> allele alone has no effect on NB6-4max, see below). To test whether *Ama* is regulated by Hox genes, we analyzed the expression of *Ama* on mRNA level using *in situ* hybridization. *Ama*-mRNA is expressed from early st10 onwards with strongest expression in a repetitive pattern at early st11 (Fig 4D) in the neuroectoderm and cells of the nervous system. At late st11, *Ama* remains strongly expressed in lateral areas, while decreasing expression in the nervous system becomes restricted to the midline (Fig 4D). Throughout the neuroectoderm we observed reduced expression in the En domain until mid st11 (Fig 4D lower panels; also [24]). Surprisingly, we found that the posterior part of the maxillary (En-expressing cells) and the anterior part of the labial segment (corresponding to parasegment 2) does not express *Ama*-mRNA, perfectly matching the *Scr* expressing region (Fig 4D lower panel, yellow box). Thus, we analyzed, whether *Scr* might repress *Ama*, and indeed in mutants for *Scr* we could observe an up-regulation of *Ama* expression in parasegment 2, the *Scr* expression domain (Fig 4E yellow box compare to Fig 4D middle lower panel, for quantification see S6B Fig). Since we find that *Ama* is a positive regulator of NB6-4max identity, this might explain why removing *Scr* has only minor effects on NB6-4max specification (10%).

Next we tested the dependency of *Ama* expression on *lab*, *Dfd* and *Antp*. Indeed, removing the function of *labial*, *Dfd* (Fig 4F), *labial/Dfd* (Fig 4G) or *Dfd/Antp* (Fig 4H) leads to a significant reduction of *Ama* expression in the corresponding segments (compare to wild type Fig 4D, middle panel, for quantification see S6B Fig). To further validate whether *Ama* is a potential transcriptional target of Hox genes, we screened the enhancer region 3kb upstream of the coding region for the existence of conserved Hox binding motifs (described in [58–61]). We could identify *Lab*, *Dfd*, *Scr* and *Antp* binding sites that are highly conserved down to *Drosophila pseudoobscura* (25–50 mio. years distance to *D. melanogaster*, S5 Fig). To show whether Hox genes actively regulate the *Ama* transcription, we ectopically expressed *Scr*, *Dfd* and *Antp* using the *scaGal4* line and monitored the *Ama* mRNA expression using *in situ* hybridization (S6C Fig). Whereas *Scr* or *Antp* did not influence the wild type expression of *Ama*, *Dfd* was able to strongly upregulate *Ama* expression in ectopic positions. Taken together our analysis shows that the secreted molecule *Ama* is a transcriptional downstream target of Hox genes.

Therefore, we assume that *Ama* transcriptional regulation by *Lab* and *Antp* can non-cell-autonomously influence the segmental specification of NB6-4max. In wild type *Lab*, *Dfd* and *Antp* positively regulate *Ama* expression in gnathal segments, ensuring together with the cell-autonomous function of *Dfd* the correct specification of NB6-4max. Loss of *Ama* regulation due to loss of *lab* or *Antp* function (in single and in double mutants) appears to be compensated by *Dfd* function and *Dfd*-regulated *Ama* expression. Conversely, in *Dfd* single mutants the *Lab*- and *Antp*-dependent expression of *Ama* can rescue the loss of *Dfd* function in approximately 50% of all hemisegments. Finally, in *lab/Dfd* or *Dfd/Antp* double mutants lacking all sources of *Ama* induction in the area of maxillary NB6-4 leads to an increase in the transformation rate to nearly 100%. Using antibody staining for *Ama*, we were able to recapitulate this on the protein level (Figs 4I–4K and S6E). In the wild type CNS *Ama*-protein is detectable in st10 and is strongly expressed in the *lab* expression domain (Fig 4I left panel, orange box). During st11e strong *Ama* signal also becomes detectable in the maxillary segment (area of NB6-4max, Fig 4I middle panel, red box) whereas labial/thoracic segments start expression from mid/late st10 onwards (Fig 4I). To analyze, which cells express *Ama* in the nervous system and whether the receptor *Nrt* is expressed in NBs at the required time point we performed antibody staining of *Ama* and *Nrt* proteins and could observe *Ama* and *Nrt* proteins in both neuroectodermal cells and Neuroblasts in stage 10 (S6D Fig).

In *Dfd* single mutants *Ama* is still visible in the area of NB6-4max (red box) presumably due to invading *Ama* protein from anterior and posterior sources (Fig 4J; *Lab*- and *Antp*-dependent), whereas double mutation for *Dfd/Antp* (S6E Fig) or *lab/Dfd* (Fig 4K) lead to a complete loss of the *Ama* signal in the maxillary segment (red box).

A further proof for our assumption of a non-cell-autonomous component of NB6-4max specification via the secreted protein *Ama* would be a double mutant for *Dfd* and *Ama*. In this mutant, both pathways would be depleted. Since both genes are located in close proximity in the *Antp* gene cluster on chromosome 3R, we were not able to establish a double mutant fly stock. We therefore followed an alternative approach of removing *Ama* function in a heterozygous *Dfd* situation by crossing a deficiency covering *Dfd* and *Ama* (*Df*(3R)BSC467) to the *Abl*<sup>1</sup>, *Ama*<sup>Ri</sup> allele (Fig 4L). In this transheterozygous situation of complete LoF of *Ama* and heterozygosity for *Dfd* we could observe an increase in the transformation rate to 50% (n = 50 mHs) of all hemisegments compared to 8% in *Dfd* heterozygotes (n = 50 mHs, S6G Fig) or 29% in *Ama* single mutants (Fig 4B), reflecting the synergistic effect of both pathways. Finally, we tested whether heatshock-induced expression of *Ama* in the *lab*<sup>1</sup>/*Dfd*<sup>12</sup> double mutant background can rescue the 100% penetrant transformation phenotype in NB6-4max. Indeed, inducing *Ama* expression at stage 9 rescued the transformation of NB6-4max in 40% of all analyzed hemisegments (Fig 4M).

Taken together, we show that the specification of segmental identity of NB6-4max depends on two pathways. First, *Dfd* acts cell-autonomously and removing *Dfd* function leads to a loss of maxillary identity and a transformation into labial/thoracic identity in 43% of all maxillary hemisegments. The remaining cases of correctly specified NB6-4max appear to be determined by a second *Dfd*-independent pathway, in which the secreted *Ama* protein, expressed under the control of *lab* and *Antp*, invades the maxillary segment from adjacent regions.

### Amalgam/Neurotactin act via Disabled regulating Abelson tyrosine kinase function to specify NB6-4max identity

Next, we wanted to understand how the non-cell-autonomous pathway of *lab* and *Antp* via *Ama* acts to specify the segmental identity of NB6-4max. *Ama* and its receptor Neurotactin (*Nrt*) have been identified as dominant enhancers of the Abelson tyrosine kinase (*Abl*) mutant

phenotype in axon pathfinding [23]. *Ama* bound to Nrt can potentially transduce signals to the tyrosine-phosphorylated adapter protein Disabled (Dab) that genetically acts upstream to Abl [62]. Other identified factors in the Abl pathway are the antagonist Enabled (Ena) [63] and a cooperating factor named Trio [64]. We tested all factors (Dab, Abl, Ena and Trio) for a possible role in NB6-4max specification.

Ena and Trio act downstream of Abl and were identified as cytoskeleton modulators via Actin regulation [65–67] and as such could influence NB divisions per se, e.g. in changing the mode of division (asymmetric versus symmetric). In the case of NB6-4max, we could not observe a transformation phenotype in *ena* or *trio* mutants (for both  $n = 50$  mHs; Fig 4A), and thus we assume that the cytoskeleton-associated function of Abl is not responsible for defects in NB6-4max.

Since *Ama* was found in a modifier screen of the *Abl* mutant phenotype, all available *Ama* mutants also harbor the mutant allele of *Abl*<sup>1</sup> [23] that encodes a truncated protein with residual kinase activity [68]. Testing the *Abl*<sup>1</sup> allele alone did not result in a transformation of NB6-4max ( $n = 50$  mHs; Fig 5A). Moreover, comparing the double mutant stock *Abl*<sup>1</sup>, *Ama*<sup>M109</sup> with a fly stock that includes an Abl rescue construct (*Abl*<sup>1</sup>, *Ama*<sup>M109</sup>, *Abl*<sup>+</sup>) (Fig 5B) showed the same transformation rate (both 10%; both  $n = 50$  mHs), strengthening our finding that a) *Ama*<sup>M109</sup> shows a transformation phenotype of NB6-4max and b) the *Abl*<sup>1</sup>-allele has no influence on the specification of NB6-4max. To test whether Abl kinase itself has an effect on NB6-4max specification, we analyzed the *Abl*<sup>t</sup> mutant allele that produces a protein with catalytically inactive kinase domain [68, 69]. This allele exhibited a transformation of NB6-4max in 41% of all hemisegments ( $n = 400$  mHs; Figs 4A and 5C). Additionally, analysis of the Abl kinase interacting protein Disabled (*Dab*<sup>1</sup>) mutation also showed a transformation of NB6-4max in 40% of all hemisegments ( $n = 60$  mHs; Figs 4A and 5D).

Thus, our analysis of the Hox-mediated non-cell-autonomous pathway of NB6-4max specification shows that *Ama*/*Nrt* possibly act via Dab to regulate the Abl kinase. Intriguingly, both intracellular components Dab and Abl show a similar transformation rate like *Dfd* single mutants (all approximately 40%), again arguing for the existence of a second *Dfd*-independent pathway. Accordingly, a *Abl*<sup>t</sup>, *Dfd*<sup>16</sup> double mutant indeed shows an increase in the transformation rate to 95% of all hemisegments ( $n = 150$  mHs; Fig 5E), strongly supporting our hypotheses that a) two independent, parallel pathways ensure the proper specification of the NB6-4max identity, and b) *Ama*/*Nrt* act through regulating the Abl kinase activity.

To further prove this, we wanted to assess whether the activity change of the Abl kinase can be monitored on the protein level in WT and *lab*/*Dfd*-mutants (impairing Hox and *Ama* pathway), since it was shown that Abl exhibits its kinase function when localized and concentrated at the cell cortex, whereas cytoplasmic Abl acts via a kinase-independent function [70–72]. In WT embryos at st11 (Fig 5F left panels), we can observe a cytoplasmic localization of Abl that shows cortical enhancement in a lot of NBs (white arrow heads) including NB6-4max (magenta arrow head), suggesting an active Abl kinase. This cortical localization is not observable in NB6-4max in *lab*/*Dfd* double mutants in which both pathways are disrupted (Fig 5F right panels, see also tracks of pixel intensities in lower panels). On the other hand, Abl function could impinge on *Dfd* localization or expression. We investigated *Abl*<sup>t</sup> mutants and we could observe nuclear *Dfd* expression in the glial and the neuronal precursor of transformed NB6-4max (Fig 5G). Finally, we wanted to analyze whether re-expression of Abl in the *lab*<sup>1</sup>/*Dfd*<sup>12</sup> or *Dfd*<sup>16</sup>/*Antp*<sup>7</sup> double mutant background could rescue the transformation phenotype. Indeed, using the *scaGal4* line to express *Abl* in the double mutant situation rescued the strong transformation phenotypes of NB6-4max in 20% of all hemisegments in the *lab*<sup>1</sup>/*Dfd*<sup>12</sup> or 40% in the *Dfd*<sup>16</sup>/*Antp*<sup>7</sup> mutants (Fig 5H).

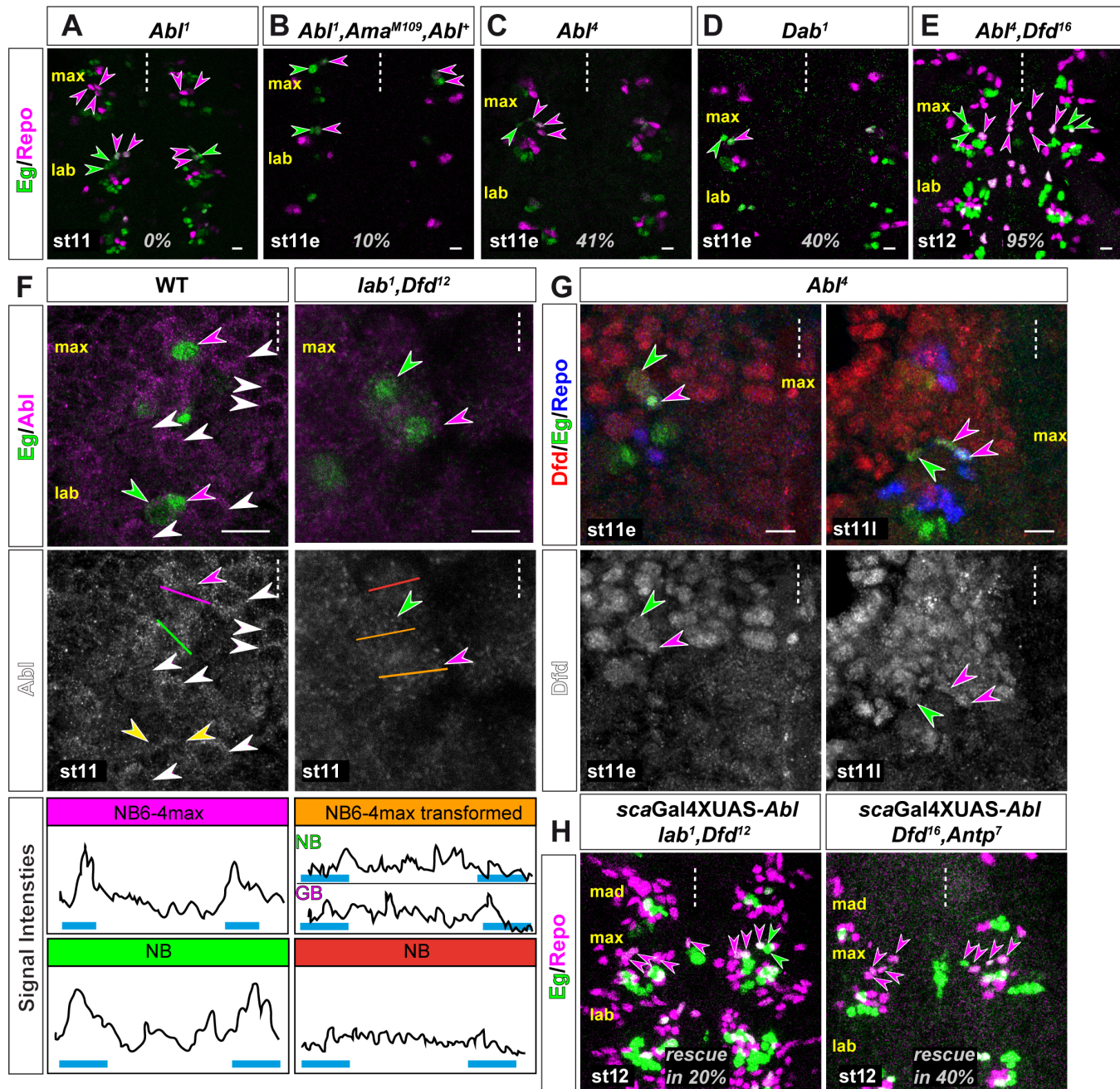


**Fig 5. Amalgam/Nrt act via Disabled regulating Abelson tyrosine kinase function to specify NB6-4max identity.** (A) Single mutation of *Abi<sup>1</sup>* shows no transformation in NB6-4max. (B) Double mutants for *Ama<sup>M109</sup>* and *Abi<sup>1</sup>* with an *Abi* rescue construct (*Abi<sup>1</sup>*) show only a minor transformation rate of 10%. (C) The mutant allele *Abi<sup>4</sup>* that has no kinase activity shows a transformation of NB6-4max in 41% of all hemisegments. (D) Mutation of the *Abi* interacting protein *Dab<sup>1</sup>* shows a transformation of NB6-4max in 40% of all hemisegments. (E) Double mutants for *Abi<sup>4</sup>* and *Dfd<sup>16</sup>* that interrupt both pathways show a transformation of NB6-4max in 95% of all hemisegments. (F) In the left panel: *Abi* (magenta) is localized in the cytoplasm with cortical enhancement in wild type NB6-4max (Eg, green; magenta arrow heads) and other NBs (white arrow heads). The labial NB6-4 has divided already (yellow arrow heads). In *lab<sup>1</sup>* and *Dfd<sup>12</sup>* (100% transformation of NB6-4max) double mutants (right panel) the cortical localization of *Abi* is disrupted. Middle panel show the *Abi* channel in monochrome. Lower panel show pixel intensity tracks of *Abi* staining across a line drawn through the cell (colors indicate corresponding line in the middle panel). In wild type (left part) NB6-4max and one other NBs as an example shows stronger pixel intensities towards the cell cortex (blue bars). This is lost in the transformed glial (GB) and neuronal precursor (NB) of NB6-4max or other NBs in the *lab<sup>1</sup>* and *Dfd<sup>12</sup>* double mutant situation (right part). (G) Transformed NB6-4 in maxillary segments of *Abi<sup>4</sup>* mutant shows normal expression of *Dfd* (red) in early st11 (left panel) and late st11 (right panel) of lineage development. Lower panel show *Dfd* channel in monochrome. (H) Re-expression of *Abi* using the *scaGal4* line rescues the transformation phenotype of NB6-4max in 20% of all hemisegments in *lab<sup>1</sup>/Dfd<sup>12</sup>* double mutants (left panel) or 40% in *Dfd<sup>16</sup>/Antp<sup>7</sup>* double mutants (right panel). Scale bar is 10  $\mu$ m.

doi:10.1371/journal.pgen.1005961.g005

Taken together, our analysis of the *Dfd*-independent pathway suggests, that *Ama/Nrt* ensure the proper specification of NB6-4max by positively regulating the kinase function of *Abl*. We conclude that nuclear located *Dfd* and cortical located *Abl* act synergistically to regulate NB6-4max identity.

Therefore, we next wanted to understand if *Dfd* and *Abl* act in parallel on the same target to ensure proper specification of NB6-4max.

### ***Dfd* and *Abl* specify maxillary identity of NB6-4 lineages by repressing *CycE***

We have previously shown, that *abdA* and *AbdB* specify abdominal (glioblast) identity of NB6-4 by repressing the cell cycle gene *CyclinE* (*CycE*), while *CycE* is expressed in thoracic NB6-4 neuroglioblasts (ground state identity) and becomes asymmetrically distributed to the neuronal daughter precursor during first division [7]. Since the loss of *Dfd* or *Abl* function leads to a transformation of NB6-4max glioblast fate into a neuroglioblast fate, we next wanted to address whether *Dfd* and/or *Abl* also modulate *CycE* expression or function. Therefore, we first studied *CycE*-mRNA expression in *Dfd*- and *Abl*-deficient NB6-4max (Fig 6A and 6B). Indeed, in transformed NB6-4max generating neurons and glial cells of *Dfd*- and *Abl*-mutants, we could observe deregulation and thus an increased expression of *CycE*-mRNA in neuronal daughter cells (Fig 6A–6C) indicating that both *Dfd* and *Abl* repress *CycE* expression in wild type NB6-4max. Furthermore, ectopic expression of *CycE* in NB6-4max was sufficient to generate a labial/thoracic neuroglioblast fate in 12% of all maxillary hemisegments ( $n = 140$  mHs; Fig 6D), whereas loss of *CycE* in labial NB6-4 leads to a loss of the neuronal sub-lineage in 64% of all hemisegments ( $n = 100$  mHs; Fig 6E), similarly to *CycE* loss in thoracic NB6-4 (Fig 6G and 6H and [7]). This shows that *CycE* is an important target in gnathal NB6-4 that has to be regulated in order to decide whether to generate neurons or not.

Since *CycE* seems to be repressed in NB6-4max by *Dfd* and *Abl*, we wanted to test, whether *Dfd* or *Abl* can repress *CycE* in labial/thoracic NB6-4 lineages, thereby repressing the ground state identity and leading to the generation of pure glial NB6-4 lineages. Ectopic expression of *Dfd* leads to a severe loss of neuronal sublineages in labial/thoracic segments in 74% of all hemisegments ( $n = 100$  Hs) and suppression of *CycE* mRNA expression in the transformed NB6-4 lineages (Figs 3H and 6E). Moreover, in the case of labial or thoracic NB6-4 expressing ectopic *Dfd*, we could observe a perfect transformation towards maxillary fate, with 4 glial cells (instead of two in abdominal hemi-segments) and no neurons. In contrast, ectopic expression of *Abl* did not result in a repression of *CycE* in labial/thoracic NB6-4 and did not lead to a transformation towards maxillary fate. This might argue for an indirect regulation of *CycE* by *Abl* through *Abl*-downstream components. If *Dfd* and *Abl* act both upstream of *CycE*, we reasoned that *CycE* should be epistatic to *Dfd* and *Abl*. Therefore, we combined the *CycE*<sup>AR95</sup> mutation with the single mutation *Dfd*<sup>11</sup> and the double mutant of *Abl*<sup>4</sup>/*Dfd*<sup>16</sup>. Indeed, loss of *CycE* leads to a rescue of the transformation phenotype in 77% of NB6-4max in *Dfd*<sup>11</sup> single mutants or 85% in *Abl*<sup>4</sup>/*Dfd*<sup>16</sup> double mutants, showing that *CycE* is epistatic to *Dfd* and *Abl* (Fig 6G and 6H).

We conclude, that both pathways ensure the proper segmental specification of NB6-4max through repression of the cell cycle gene *CyclinE*.

### ***Abl* seems to regulate *CycE* expression via the Hippo/Salvador/Warts pathway**

Since *Abl* is a cytoplasmically/cortically localized kinase, we next wanted to address how *Abl* might repress *CycE* transcription. In addition to the higher proliferation rate of NB6-4max in

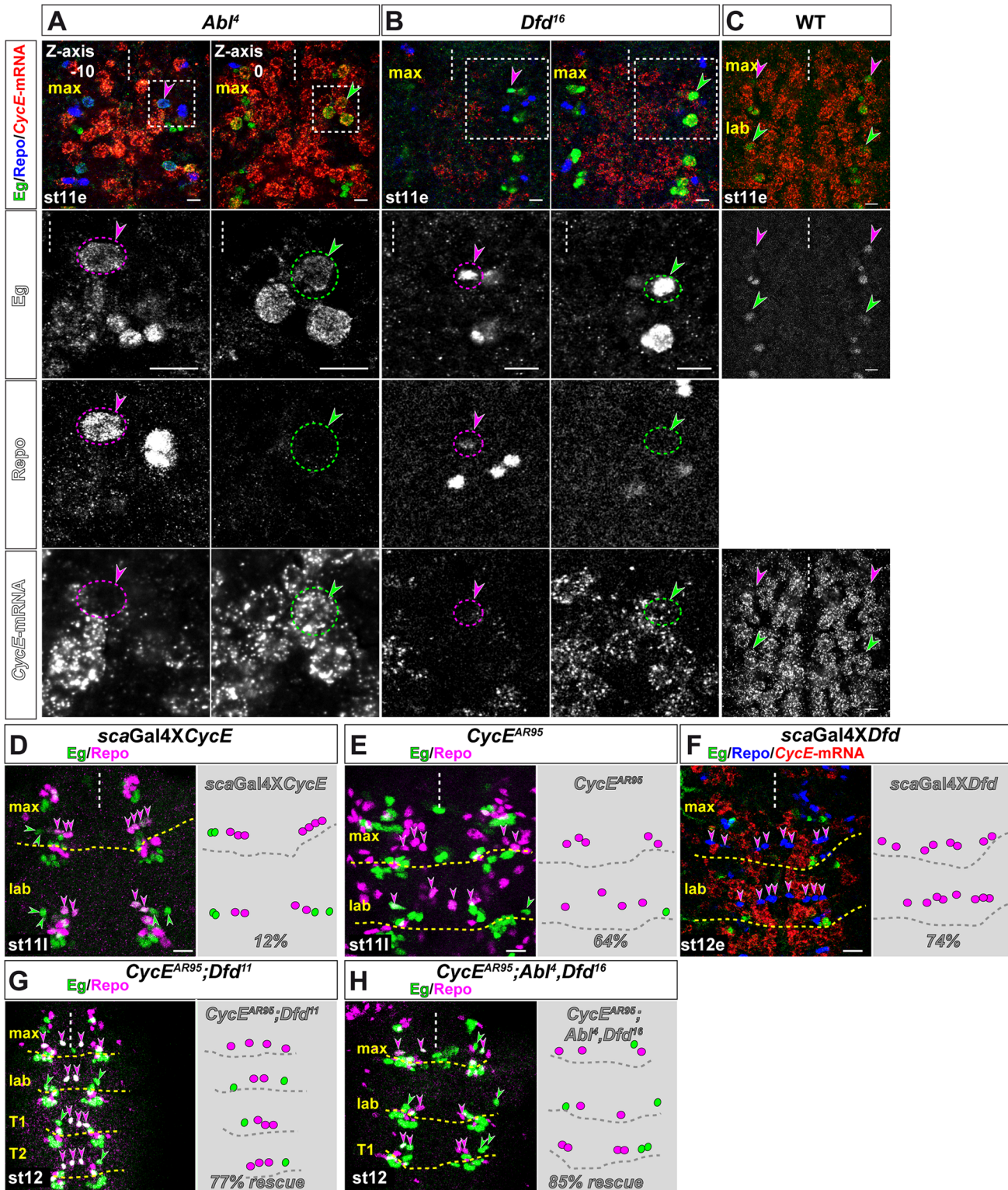


**Fig 6. Dfd and Abl specify maxillary identity of NB6-4 lineages by repressing CycE.** (A, B) In *Abi<sup>4</sup>* (A) as well as in *Dfd<sup>16</sup>* (B) mutant NB6-4max *CycE* is de-repressed and becomes distributed to the neuronal part of the transformed lineage. Whereas after the first division the glial daughter precursor (magenta circles and arrow heads, left panels) shows no *CycE* mRNA (red) the neuronal daughter precursor (green circles and arrow heads, right panels) shows clear *CycE* mRNA staining. (C) Wild type expression of *CycE* mRNA in the maxillary (magenta arrow heads) and labial NB6-4 (green arrow heads). In the maxillary segment only very weak expression of *CycE* mRNA can be found in NB6-4, whereas the labial NB6-4 shows a strong *CycE* mRNA expression. (D) Ectopic



expression of *CycE* using the *scabrous-Gal4* (*scaGal4*) line transforms maxillary NB6-4 glioblast fate into labial/thoracic neuroglioblast fate in 12% of all hemisegments. (E) Mutation of *CycE*<sup>AR95</sup> shows loss of the labial NB6-4 fate with only glia cells produced in 64% of all labial hemisegments. (F) Ectopic expression of *Dfd* using the *scabrous-Gal4* (*scaGal4*) line transforms labial/thoracic NB6-4 into a maxillary fate, generating four glial cells and no neuronal cells in 74% of all thoracic hemisegments. At this stage (st12e) no *CycE* mRNA (red) is observable in NB6-4 derived glial cells. (G) Loss of *CycE* in the *Dfd*<sup>11</sup> single mutant leads to a rescue of the transformation phenotype of NB6-4max in 77% of all hemisegments. *CycE*<sup>AR95</sup> mutation also leads to the loss of neuronal cells in the thoracic segments. (H) Loss of *CycE* in the *Abl*<sup>d</sup>, *Dfd*<sup>16</sup> double mutants leads to a rescue of the transformation phenotype of NB6-4max in 85% of all hemisegments. Scale bar is 10  $\mu$ m.

doi:10.1371/journal.pgen.1005961.g006

*Abl* mutants (4–5 neurons and 3 glial cells versus 4 glial cells in the wild type), we observed a statistically significant increase in nuclear size (S7A–S7C Fig) of the Eg-positive NBs in gnathal segments. A number of *Abl* mutant embryos displayed an overproliferation phenotype with many supernumerous Eg-positive cells at the end of embryogenesis (S7D–S7F Fig). To circumvent the problem of second site mutations on the mutant chromosome, we also tested transheterozygous mutations and could observe similar results in different allelic combinations (S7A and S7B Fig). Interestingly, the same phenotype could be observed in *lab/Dfd* double mutants (S7G Fig), also disrupting the *Ama/Abl* pathway, or *Nrt*<sup>1</sup> mutants (S7H Fig), but never in any of the single Hox mutants, in which *Abl* function is normal. Since this implies that *Abl* might regulate a pathway involved in proliferation and growth affecting *CycE*, and since a possible connection of the vertebrate homologue c-*Abl* with the Hippo/YAP pathway was recently suggested [73, 74], we wondered whether the highly conserved Hippo/Salvador/Warts (HSW) pathway might be involved in this process. At the center of the HSW pathway are the two core kinases Hippo (Hpo) and Warts (Wts) that phosphorylate and thereby inhibit the transcriptional regulator Yorkie (Yki) [75–77]. When Hpo is active it phosphorylates Salvador (Sav) that becomes stabilized [78, 79] and leads to the phosphorylation of the downstream kinases Mats and Wts. Wts finally phosphorylates Yki that upon phosphorylation remains in the cytoplasm and is inactive [80]. As soon as Hpo/Wts are inactive, Yki is no longer phosphorylated and can enter the nucleus, complex with other transcription factors like Scalloped (Sd) and start transcription of its target genes like *CycE* [80, 81].

Since so far the HSW pathway has not been implicated in embryonic NBs development, we first wanted to show the presence of the active Hpo kinase in early *Drosophila* NBs. One way to monitor Hpo activity in tissues is the Salvador (Sav) protein, since Sav is stabilized only in the presence of active Hpo via phosphorylation, whereas absence of Hpo or loss of Hpo activity leads to the destabilization of Sav and its subsequent targeting for degradation [78, 79]. We used antibody staining to visualize the levels of Sav. In wild type we can find a strong staining for Sav in nearly all embryonic NBs (Fig 7A) suggesting an active Hpo kinase. Moreover, active Hpo should lead to the cytoplasmic retention of Yki, and indeed using antibody staining, we could observe a predominant cytoplasmic localization of Yki in NB6-4max with only minor signal in the nucleus, prior to its first division (Fig 7D). Next we tested, whether Hpo activity is impaired in *Abl*-single (Fig 7B) or *lab/Dfd*-double mutants (Fig 7C). We were not able to monitor Yki nuclear localization in the mutant situation, but observed a clear reduction of the Sav protein (Fig 7B and 7C), suggesting that the loss of *Abl* function might lead to the destabilization and degradation of Sav. Since it was shown that c-*Abl* phosphorylates and activates vertebrate MST1 and MST2 (homologues of Hpo) and *Drosophila* Hpo [74], the loss of Sav in the *Abl* LoF situation implies an inactive Hpo kinase.

Although we were not able to show a change in the subcellular localization of Yki, we still wanted to examine the function of Yki in NB6-4max lineage development. To test if Yki is sufficient to generate neurons in NB6-4max and therefore to transform its identity, we ectopically expressed a constitutive active form of Yki (*Yki*<sup>S168A</sup>, *Yki*<sup>CA</sup>) [82] (Fig 7E). This Yki protein can no longer be phosphorylated by Warts and as such is nuclear and active [82]. Expression of

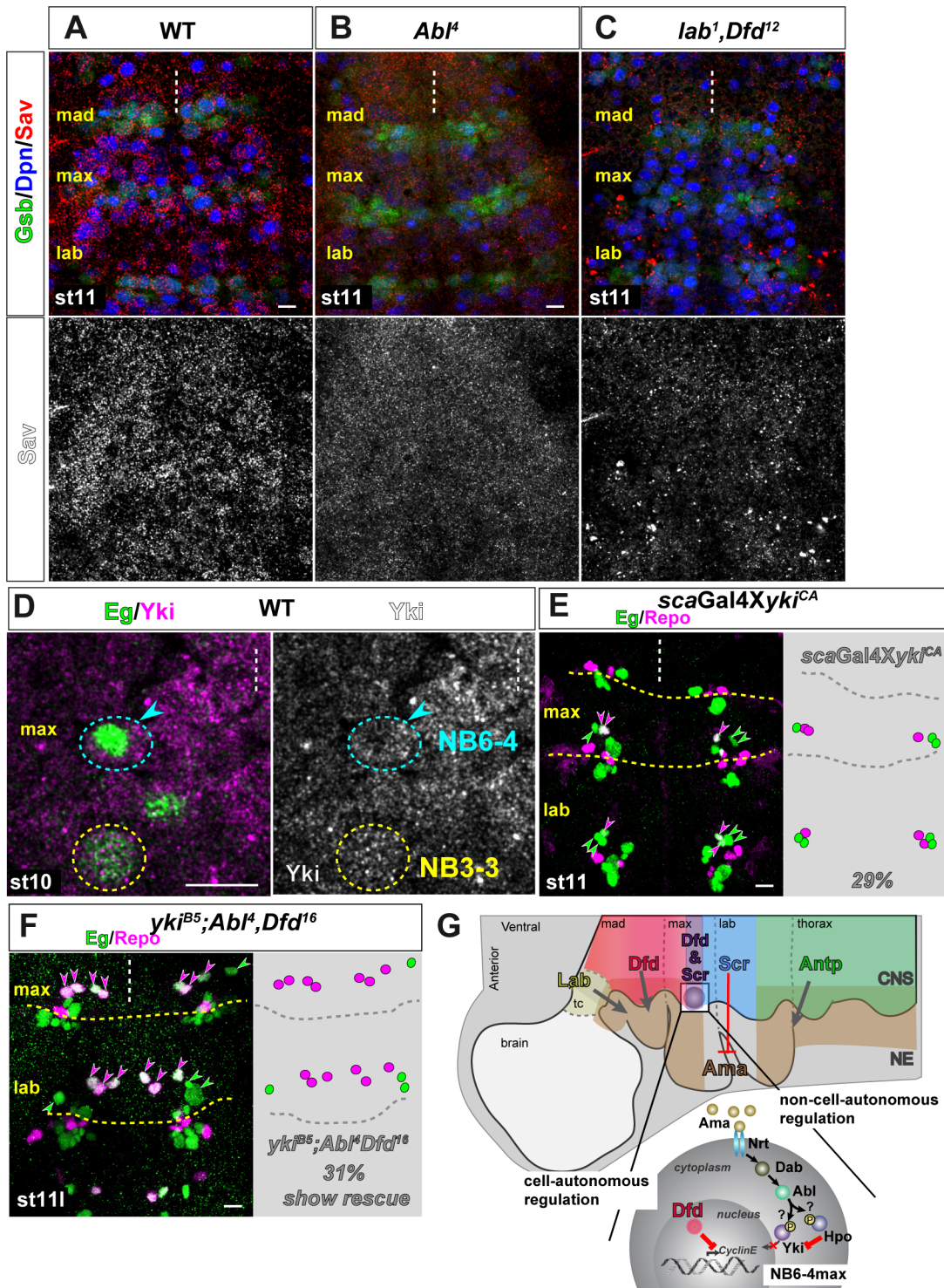


**Fig 7. *Abi* potentially regulates *CycE* expression via the Hippo pathway.** (A-C) In wild type neuroblasts stained with Dpn (blue) at stage 11 (A) a stable expression of Salvador (Sav, red) can be observed mirroring the active Hpo kinase. Mutation in *Abi<sup>4</sup>* (B) or double mutation in *lab<sup>1</sup>* and *Dfd<sup>12</sup>* (C) show reduced Sav protein distribution, which argues for a less stable protein and an inactive Hpo kinase. Lower panel shows Sav channel in monochrome. (D) Yorkie (magenta) is localized to the cytoplasm of NB6-4max prior to its first division at stage 10. Cytoplasmically localized Yki is the inactive form of Yki. (E) Ectopic expression of a constitutive active form of *Yki<sup>CA</sup>* using the *scabrous*-Gal4 (*scaGal4*) line transforms NB6-4max in 29% of all maxillary hemisegments. (F) Triple mutation for *yki<sup>B5</sup>* and *Abi<sup>4</sup>, Dfd<sup>16</sup>*, shows a decrease in the transformation rate from 100% in the double mutants for *Abi<sup>4</sup>, Dfd<sup>16</sup>* to 69% in the triple mutants. Thus, the loss of *yki* rescues the double mutant phenotype in 31% of all hemisegments. (G) Schematic model of the cell-autonomous and non-cell-

autonomous regulation of maxillary identity specification of NB6-4. Expression pattern of Antp-C genes are shown color-coded in the CNS. In the posterior part of the maxillary segment Dfd and Scr are co-expressed. Lab, Dfd and Antp positively regulate the expression of Ama (brown areas and arrows), whereas Scr represses Ama expression. Ama binds to Nrt and via Dab activates Abl that leads to the repression of CycE expression presumably through the Hippo/Salvador/Warts pathway. Whether Abl influences the Hpo kinase or Yki itself needs to be further clarified. Scale bar is 10  $\mu\text{m}$ .

doi:10.1371/journal.pgen.1005961.g007

$Yki^{CA}$  leads to a phenocopy of the  $Abl^4$  mutant phenotype, with NB6-4max transformed to a thoracic/labial identity in 29% ( $n = 60$  mHs; Fig 7E) and a general increase in nuclear sizes and cell proliferation (S71 Fig). Finally, we tested the effect of  $yki^{B5}$  mutation alone or in combination with  $Abl^4/Dfd^{16}$  or  $lab^1/Dfd^{12}$  mutants.  $Yki^{B5}$  mutants are predominantly embryonic lethal, but a few escapers also develop into larvae. In  $yki^{B5}$  single mutants we could not observe a loss of neuronal cells in labial or thoracic segments ( $n = 25$  mHs). Nevertheless, double or triple mutants for  $yki^{B5}$  and  $Abl^4/Dfd^{16}$  or  $yki^{B5}$  and  $lab^1/Dfd^{12}$  (both  $n = 35$  mHs; Figs 7F and S71) showed a rescue of the transformation phenotype in 31% or 34%, respectively (a drop from 100% transformation to 69% or 66%, respectively). This indicates that Yki is necessary for the generation of neurons in the transformed NB6-4max of  $Abl^4/Dfd^{16}$  or  $lab^1/Dfd^{12}$  mutants, and suggests that Abl kinase specifies NB6-4max identity potentially by activating the HSW pathway and thereby repressing the expression of *CycE*.

## Discussion

Along the anterior-posterior axis the CNS consists of segmental units (neuromeres) the composition of which is adapted to the functional requirements of the respective body parts. In *Drosophila* the CNS comprises 10 abdominal, three thoracic, three gnathal and four pregnathal (brain) neuromeres that are generated by stereotyped populations of neural stem cells (neuroblasts, NBs). The pattern of NBs in thoracic segments resembles the ground state while NB patterns in the other segments are derived to various degrees [14, 17]. Within each segment individual NBs are specified by positional information in the neuroectoderm [83, 84]. NBs delaminating from corresponding positions in different segments express similar sets of molecular markers [2, 14], generate similar lineages, and are called serial homologs. However, for thoracic and abdominal neuromeres it has been shown that the composition of a number of serially homologous NB-lineages shows segment-specific differences [4, 6, 85]. In the more derived gnathal and pregnathal head segments embryonic NB-lineages and the mechanisms of their segmental specification have not been analyzed so far.

### Identification of serially homologous NB-lineages exhibiting segment-specific differences in gnathal segments

Using the well-established molecular marker Eagle (Eg) which labels four embryonic NB-lineages (NB2-4, NB3-3, NB6-4, NB7-3) in all thoracic and most of the abdominal segments [20, 21] we identify serially homologous lineages of NB3-3, NB6-4 and NB7-3 in gnathal segments. The embryonic NB7-3 lineage shows segmental differences as it comprises increasing cell numbers from mandibular (2 cells), maxillary (3 cells) to labial (3–5 cells) segments, while cell numbers are decreasing from T1-T2 (4 cells), T3-A7 (3 cells) to A8 (2–3 cells) [14, 35]. Reduced cell numbers in the mandibular and maxillary NB7-3 lineages depend on Dfd and Scr function, respectively (S8A–S8E Fig). While NB7-3 appeared in all three gnathal segments, NB3-3 and NB6-4 was only found in labial and maxillary segments, and NB2-4 was not found in any of them. Our preliminary data suggest that the missing NBs are not generated in these segments, instead of being eliminated by apoptosis. For the terminal abdominal neuromeres (A9, A10) it has recently been shown that the formation of a set of NBs (including NB7-3) is inhibited by the Hox gene *Abdominal-B* [13]. Similarly, in *Dfd* mutants we occasionally

observed the formation of a NB with NB6-4 characteristics in mandibular segments (10%, [S8F Fig](#)), in which it is never found in wild type.

Similar to the thoracic and abdominal segments [6] NB6-4 showed dramatic differences between maxillary and labial segments. NB6-4max produces glial cells only (like abdominal NB6-4), whereas the labial homolog produces neurons in addition to glial cells (like thoracic NB6-4). The number of glial cells produced by the glioblasts NB6-4max (4 cells) and abdominal NB6-4 (2 cells) and by the neuroglioblasts NB6-4lab (3 glia) and thoracic NB6-4 (3 glia) is segment-specific.

Thus segment-specific differences among serially homologous lineages may concern types and/or numbers of specific progeny cells and may result from differential specification of NBs and their progeny, differential proliferation and/or differential cell death of particular progeny cells. It has been shown that the segment-specific modification of serially homologous lineages is under the control of Hox genes and that during neurogenesis Hox genes act on different levels, i.e. they act in a context-specific manner at different developmental stages and in different cells (reviewed in [86]). In the thoracic/abdominal region segmental identity is conferred to NBs early in the neuroectoderm by cell-autonomous function of Hox genes of the Bithorax-Complex [8, 9, 46]. In this study we used the NB6-4 lineage to clarify mechanisms of segmental specification in the gnathal segments.

### Serially homologous NB6-4 lineages in gnathal segments are defined by cell-autonomous and non-cell-autonomous function of Antp-C genes

In segments of the trunk, the action of Hox genes strictly follows the rule of the posterior prevalence concept [12, 87]: More posterior expressed Hox genes repress anterior Hox genes and thereby determine the segmental identities. In the gnathal segments we could not observe this phenomenon on the level of the nervous system. Removing Hox genes of the Antp-C had no or only minor impact on the expression domain of other Antp-C Hox genes (see [S4 Fig](#)). Similar results were also obtained in a study that analyzed cross-regulation of Hox genes upon ectopic expression [88].

Moreover, it seems that at least in the case of the differences monitored between labial and maxillary segments Hox gene function has to be added to realize the more anterior fate. Antennapedia has no impact on NB6-4 identity in the labial segment, but specification of the maxillary NB6-4 requires the function of Deformed and Sex combs reduced. These two Hox genes are not repressed or activated by Antp (see also [88]). Also, cross-regulation between Dfd and Scr seems to be unlikely or is very weak since we observed only mild effects on the protein level and on the phenotypic penetrance. In principle Scr can repress *Dfd*, but it was suggested that this occurs only when products are in sufficient amounts [89]. In NB6-4 Dfd and Scr are co-expressed, but Scr levels appear to be insufficient to repress *Dfd*. *Dfd* seems to be the major Hox gene that cell-autonomously confers the maxillary NB6-4 fate, since the loss of *Dfd* showed the highest transformation rate and, more importantly, ectopic expression of *Dfd* in thoracic segments leads to a robust transformation towards maxillary fate. Scr does not act redundantly since in double mutants *Dfd/Scr* we did not find a synergistic effect. It might have a fine-tuning effect, as we could show that Scr influences *Ama* by repressing its transcription, whereas all other Antp-C Hox genes seem to activate *Ama*. However, since we could find only minor changes in cell identities and numbers in *Scr* LoF background, the role of Scr in NB6-4max stays enigmatic.

To our surprise cell-autonomous Hox gene function was not the only mechanism that confers segmental identity in NB6-4max. Loss of *Dfd* showed an effect in approx. 43% of all segments. Moreover, mutations of the adjacently expressed Hox genes *labial* and *Antennapedia* in

combination with *Dfd* LoF showed a dramatic increase in the transformation rate of NB6-4max. We carefully studied their expression patterns on the mRNA and protein level in wild type and Hox mutant background. In no case we could find these genes to be expressed in NB6-4max or in the neuroectodermal region from which NB6-4max delaminates. This indicates that *labial* and *Antennapedia* influence NB6-4max fate in a non-cell-autonomous manner. That Hox genes can act non-cell-autonomously on stem cells was recently shown in the male germ-line, where *AbdB* influences centrosome orientation and the proliferation rate through regulation of the ligand *Boss* in the *Sevenless*-pathway [90]. In our study *Antp-C* Hox genes control the expression of the secreted molecule *Amalgam*, which spreads to adjacent segments and ensures segmental specification of NB6-4max in a parallel mechanism to the cell-autonomous function of *Dfd*. Thus, we provide first evidence for parallel non-cell-autonomous and cell-autonomous functions of *Antp-C* genes during neural stem cell specification in the developing CNS.

### The role of Abelson kinase in NB specification

Abelson kinase (*Abl*) was shown to be required for proper development of the *Drosophila* embryonic nervous system. In neurons *Abl* interacts with proteins like *Robo* [91] or *Chickadee* [92] and influences the actin cytoskeleton in the growth cone [93] to regulate axonogenesis and pathfinding. In this system it was also demonstrated that *Ama* and *Nrt* are dominant modifiers of the *Abl* phenotype [23]. In our model (Fig 7G) we propose that the interaction of secreted *Ama* and the membrane-bound *Nrt* regulates *Abl* function in NBs. This leads to the correct segmental specification of NB6-4max. *Antp-C* Hox genes *lab*, *Antp* and *Dfd* regulate the expression of *Ama* and in mutants for these Hox genes expression of *Ama* is severely reduced, which leads to the transformation of NB6-4max due to missing *Abl* function and de-repression of the cell cycle gene *CyclinE*. That *Abl* can influence the expression of *CyclinE* was also demonstrated in a modifier-screen in the *Drosophila* eye, but the mechanism remained unclear [94]. Our genetic analysis now suggests that in NBs this might occur via the regulation of the highly conserved HSW pathway [75–77] and its downstream transcriptional co-activator *Yki*, which is known to regulate *CyclinE* expression [80]. The HSW pathway controls organ growth and cell proliferation in *Drosophila* and vertebrates but so far has not been implicated in embryonic NB development. We could observe *Yki* cytoplasmic localization in wild type NB6-4max prior to division suggesting the active Hippo pathway. Although we could not detect nuclear localization of *Yki* in *Abl* mutants, the loss of *Yki* activity in the *Abl* mutant background leads to a significant reduction in the strength of the *Abl* single mutant phenotype showing their genetic interaction and therefore supporting our proposed model in which *Abl* influences *Yki* activity. Moreover, expression of constitutive active *Yki* also lead to the transformation of NB6-4max and phenotypes that were similar to those observed in *Abl* mutants. We tried to assess how *Abl* might influence *Yki* activity. Work in vertebrates suggests that this could be at least on two levels: first, c-*Abl* was shown to directly phosphorylate and activate the vertebrate *MST1* and *MST2* (*Hpo* homologue) and the *Drosophila* *Hpo* on a conserved residue (Y81) [74] and second, c-*Abl* can also phosphorylate *YAP1*, which changes its function to become pro-apoptotic [73]. Our analysis suggests that in NBs *Abl* might regulate *Hpo*, since we could find changes in the stability of *Salvador*, which is used as a *Hpo* activity readout [78, 79], but we can not rule out a parallel direct regulation of *Yki*, since it was recently shown that other pathways like the *AMPK/LKB1* pathway can directly influence *Yki* activity [95, 96]. Since we could observe severe over-proliferation in *Abl* or *lab/Dfd* mutants, that have an impaired *Ama-Nrt-Abl* pathway, or upon overexpression of *Yki*<sup>CA</sup>, future studies need to

elucidate whether and how the proto-oncogene Abl kinase and Hox genes act on growth and proliferation or even tumor initiation through regulation of the Hippo/Salvador/Warts pathway.

## Materials and Methods

### Fly stocks

*Oregon R* (used as wild type), *lab*<sup>4</sup>, *pb*<sup>17</sup>, *Scr*<sup>11</sup>, *Scr*<sup>17</sup>, *Dfd*<sup>11</sup>, *Dfd*<sup>12</sup>, *Dfd*<sup>16</sup>, *Antp*<sup>25</sup>, *Antp*<sup>11</sup>, *Dfd*<sup>16</sup>/*Scr*<sup>4</sup>, *Dfd*<sup>16</sup>/*Antp*<sup>7</sup>, *lab*<sup>1</sup>/*Dfd*<sup>12</sup>, *Scr*<sup>4</sup>/*Antp*<sup>25</sup>, *CycE*<sup>AR95</sup>, *Abl*<sup>4</sup>, *Abl*<sup>1</sup>, *Nrt*<sup>1</sup>, *hd*<sup>Ef</sup>, *disco*<sup>1</sup>, *dpp*<sup>hr27</sup>, *ems*<sup>4</sup>, *Dab*<sup>1</sup>, *ena*<sup>23</sup>, *trio*<sup>8</sup>, *sas4*<sup>s2214</sup>, *grappa*<sup>61A</sup>, *zen*<sup>1</sup>, *bcd*<sup>12</sup>, *ftz*<sup>11</sup>, *Alh*<sup>r13</sup>, *wg*<sup>8</sup> (all strains are balanced with *TM6b*), *iab2-lacZ Antp-Hu e*, UAS-*CyclinE*, UAS-*n-lacZ*, UAS-*ykiS168A* (*yki*<sup>CA</sup>), *sca-brous-Gal4*, *engrailed-Gal4*, Hsp70-*Ama*, UAS-*Abl* (all from Bloomington); *Ama*<sup>M109</sup>/*Abl*<sup>1</sup>, *Ama*<sup>M109</sup>/*Abl*<sup>1</sup>, *Abl*<sup>+</sup> *Ama*<sup>R1</sup>/*Abl*<sup>1</sup> and *Nrt*<sup>M54</sup>/*Abl*<sup>1</sup> (gifts from E. Liebl) [23]; *tsh/tio*<sup>8</sup> and *tsh*<sup>2757</sup> (gifts from L. Fasano) [97–99], *yki*<sup>B5</sup> (gift from J. Knoblich, [80]), *gbb*<sup>1</sup> and *gbb*<sup>2</sup> (gifts from K. Wharton) [100], *mspo*<sup>c26</sup> (gift from A. Nose) [101], *wg*<sup>cx4</sup> (gift from J. Ng) [102], UAS-*Dfd*, UAS-*Scr*, UAS-*Antp*, UAS-*lab* (gifts from A. Percival-Smith) [88, 103–105].

### In silico binding sites for Hox genes

To identify conserved Hox binding sites in the *Ama* locus we used the EvoPrinterHD (<http://evoprinter.ninds.nih.gov/>) and compared *Drosophila melanogaster* to *Drosophila pseudoobscura* and *Drosophila simulans*. Entry sequence was the *D. melanogaster Ama* gene locus plus 3kb of upstream sequence from the 5'UTR of Flybase release 2015\_01.

### Immunocytochemistry

Following dechorionization in 7.5% bleach, embryos from overnight collections were devitelled and fixed in heptane with 4% formaldehyde in 0.3% PBT buffer (1x PBS with 0.3% Triton, C. Roth) for 20 minutes. Dechorionisation and dehydration was accomplished by vortexing and 10 min wash in methanol. The heatshock of Hsp70-*Ama* in *lab*<sup>1</sup>/*Dfd*<sup>12</sup> double mutants was induced at embryonic stage 9 for 1 hour at 37°C. Afterwards embryos were allowed to develop until stag 13 at 25°C before fixing and staining.

Primary antibodies used: mouse (m) α-Eg (1:100, gift from C.Q. Doe) [106], rabbit (rb) α-Eg (1:500) [20], rb α-Repo (1:500, gift from T. Halter) [37] and guinea pig (gp) α-Repo (1:1000, gift from B. Altenhein) [107], gp α-Dfd (1:100, gift from W. McGinnis) [108], rb α-En (1:100), rb α-Dfd (1:20, both Santa Cruz), m α-Engrailed (1:5), m α-Nrt (1:100), m α-Ena (1:1000), m α-Dab P4 (1:50), m α-Wrapper (1:20), m α-Antp (1:20), m α-Scr (1:20), m α-Prospero (1:10, all DSHB), rb α-Pb (1:50, gift from T. Kaufman) [109], rat α-Lab (1:10, gift from F. Hirth) and rb α-Lab (1:100, gift from H. Reichert), rb α-Ama (1:500, gift from I. Silman) [25], rb α-Abl (1:500, gift from E. Giniger) [62], m α-beta-gal (1:750, Promega), chicken α-beta-gal (1:1000, Cappel), rb α-Castor (1:500, gift from M. Odenwald) [110], m α-GFP (1:500, Covance), rat α-Gooseberry distal and rat α-Gooseberry proximal (1:2, gift from R. Holmgren) [111], gp α-Zfh1 (1:500), gp α-Deadpan (1:1000, both gift from J. Skeath), gp α-Runt (1:500, gift from J. Reinitz) [112], rb α-Ey (1:1000, gift from Uwe Walldorf) [34], rb α-Ind (1:3000, gift from T. von Ohlen) [113], rb α-Yki (1:200, gift from K. Irvine) [82], rb α-Sav (1:100, gift from J. Jiang) [114], rb α-pH3 (1:1000, Abcam).

The secondary antibodies used were α-mouse-Cy3, α-rabbit-FITC, α-rabbit-Cy3, α-guinea pig-Cy5, α-rat-Cy5 (1:500, all from donkey, all Jackson Immunoresearch Laboratories) and donkey α-mouse-Alexa488 (1:500, Molecular Probes).

In situ probes against *Ama*-, *Dfd*-, *Scr*-, *Antp*-, *gcm*- and *CycE*-mRNA were generated by PCR using the DIG-RNA and FITC-RNA labeling kit (Roche Applied Science) from an embryonic cDNA library and genomic DNA. The probe for *labial*-mRNA was generated by R. Urbach. In situ hybridizations were performed according to standard procedures using a 40% formamide hybridization solution.

The Leica TCS SP2 and SP5 confocal microscope was used for fluorescent imaging, and images were processed using Leica Confocal software, Adobe Photoshop and Adobe Illustrator. Pixel intensities and tracks of pixel intensities were measured using the Volocity software. Statistical analysis of the nuclear size was analyzed using the sigmaBlot v.11 software.

## Measurement of Hox gene expression domains

Embryos from stage 5 to stage 9 (according to Campos-Ortega and Hartenstein 1997) where stained with Alkaline Phosphatase (AP) and *in-situ* RNA-probes for *lab*, *Dfd*, *Scr* and *Antp* mRNA. Whole-mount embryos where documented with a Zeiss Axioplan microscope using a 40x objective and pictures where digitalized with a Kontron Progress3012 camera. The measurements of the Hox gene expression domains were taken with the Adobe Photoshop CS4 measurement tool. The total length of the embryo was taken as 100% value and the extent of the expression domain calculated accordingly from the anterior pole. All single values where evaluated statistically with Microsoft Excel to attain a median for each stage and Hox gene.

## Supporting Information

**S1 Fig. Identification of Eg-expressing cells in the gnathal segments.** (A) Triple-staining for Eg (green), Gsb (red) and Even-skipped (Eve, blue) identifies the Eve-positive progeny of NB3-3. Right panel shows Eve and Gsb staining only. White arrows indicate the position of NB3-3 cell lineage. (B) Double staining for Eg (green) and Eyeless (Ey, magenta) identifies NB7-3 cell lineage (white arrows). (C) In labial segments NB6-4 divides asymmetrically and Prospero (Pros, magenta, upper panel) and the *gcm*-mRNA (magenta, lower right panel) are unequally distributed during the first division to the glial precursor (magenta arrow head). *Gcm*-mRNA in the maxillary NB6-4 is distributed to both daughter cells during the first division (lower left panel). (D) At stage 16 many more cells express Eg compared to thoracic or abdominal segments. (E-K) Identification of midline cells based on expression of the markers (all shown in magenta) Single-minded (Sim, E) [41], Runt (F), Engrailed (En, G), Castor (Cas, H), Zinc finger homeodomain 1 (Zfh-1, I), Wrapper (J) and Pros (K). The Eg-positive midline cells (white circles) have been identified as progeny of the MNB [42]. (L-O) Identification of ventrally located clusters of Eg-positive cells (white circles) as progeny of the NB 5–3 using the marker proteins (all in red) Runt (L), Ey (M), Ladybird-early (Lbe, N) and Intermediate nervous system defective (Ind, O). Since these cells express Gsb but not En, they seem to derive from row 5 NBs (L)[32, 43]. The expression of Runt (NB5-2 and NB5-3)[29] in combination with Eyeless (NB5-3), Ladybird (NB5-3 progeny and NB5-6)[44] or Intermediate-nervous-system-defective (Ind, NB5-3)[45] indicate that these cells derive from NB5-3 (L-O). Scale bar is 10 μm. (TIF)

**S2 Fig. Detailed expression analyses reveal late progeny of NB6-2, NB4-3, NB4-4 and NB5-6 in the maxillary and/or the mandibular segments as extra Eg-positive cells.** (A) Identification of extra Eg-positive cells (green) in the mandibular segment at stage 14. Markers used are shown in red: Ey, Ming, Hucklebein (Hkb), Empty spiracles (Ems) and muscle segment homeobox (Msh). The combination of marker expression of Ey, Ming, Hkb in addition to Ems labels NB4-4 (yellow arrow heads), and in addition to Msh labels NB4-3 (cyan arrow heads).

(B) Identification of extra Eg-positive cells (green) in the maxillary segment at stage 14. Markers used are shown in red, Ey, Ming, Hkb, Lbe, Ind, Dachshund (Dac) and Msh. Expression of Ey, Msh, *ming-lacZ*, *hkb-lacZ* and Dac and missing expression of Gsb labels NB4-3 (white circle). The combination of Lbe and Gsb and missing expression of Ey labels NB5-6 (cyan circle). NB6-2 is identified by expression of Eg, Gsb and Ind (blue circle). NB5-3 Eg-positive cells (yellow circle) are identified by expression of Gsb, Lbe, Ey, *ming-lacZ* and *hkb-lacZ*. Scale bar is 10  $\mu$ m.

(TIF)

**S3 Fig. Measurements of the expression domains of *labial*-, *Deformed*-, *Sex combs reduced*- and *Antennapedia*-mRNA at stages 5, 6, 7 and 8.** For each stage and corresponding gene the measurements for several embryos are shown. The width of the expression domain is represented by a red bar for each individual embryo and its position is given in percent of the egg length. Along a representative image is given. The bottom panel shows the average expression domains of all analyzed genes per stage. Scale bar is 10  $\mu$ m.

(TIF)

**S4 Fig. Influence of Hox genes on NB6-4max and *Hox* gene expression pattern in Hox gene mutants.** (A) Ectopic expression of *Scr* using the *scabrousGal4* (*scaGal4*) line does not alter labial NB6-4 segmental identity. (B) Ectopic expression of *Dfd* using the *scaGal4* line transforms labial NB6-4 (neuroglioblast) into a NB6-4max (glioblast) identity in 74% of all hemisegments. (C) In *labial<sup>4</sup>* (*lab<sup>4</sup>*) mutants no transformation of NB6-4max can be observed—the lineage comprises four glial cells (magenta arrow heads) and no neuronal cells. (D) In *lab<sup>1</sup>* and *Antennapedia<sup>25</sup>* (*Antp<sup>25</sup>*) double mutants no transformation of NB6-4max can be observed—four glial cells (magenta arrow heads) and no neuronal cells are present. (E) In *lab<sup>1</sup>* and *Dfd<sup>12</sup>* double mutants NB6-4max is transformed into a mixed lineage distributing *gcm*-mRNA (magenta) to the glial sublineage, revealing a transformation on the progenitor level. (F) Double mutation of *Scr<sup>4</sup>* and *Antp<sup>25</sup>* leads to an increase in the transformation rate of NB6-4max (33%) compared to single *Scr<sup>17</sup>* mutants (10%). (G) Expression pattern of *Dfd*, *Scr*, *Antp* and *Lab* (all in magenta) in the wild type nervous system at the indicated stages. Stainings are either in combination with Eg or En (green). (H) Expression of *Lab*, *Scr*, *Antp* (magenta, *Scr* also in red) or *Scr*-mRNA (red) in *Dfd<sup>16</sup>* mutants. *Scr* protein is reduced, which is presumably due to a translational inhibition as we observed normal mRNA (right panel) levels. Lower panels show *Scr* or *Scr*-mRNA channel alone. (I) Expression of *Dfd* and *Antp* (both magenta) is not altered in *Scr<sup>11</sup>* mutants. (J) Expression of *Scr* (magenta) is not altered in *Antp<sup>25</sup>* mutants. (K) Expression of *Scr*-mRNA (red) and *Antp* (green) is not altered in *lab<sup>1</sup>Dfd<sup>12</sup>* double mutants. (L) Expression of *Lab* (red) and *Antp* (green) is not altered in *Dfd<sup>16</sup>Scr<sup>4</sup>* double mutants. (M) Expression of *Dfd* (magenta) is not altered in *Scr<sup>17</sup>Antp<sup>25</sup>* double mutants. (N) Expression of *Scr* (magenta) is not altered in *lab<sup>4</sup>* mutants. (O) Proboscipedia (red) is not expressed in NB6-4. Scale bar is 10  $\mu$ m.

(TIF)

**S5 Fig. Hox binding sites are conserved in the *Ama* gene locus of *Drosophila melanogaster*, *D. simulans* and *D. pseudoobscura* (25–55 Million years).** Conserved binding sites in all three species are shown in black capital letters.

(PDF)

**S6 Fig. *Ama* transcriptional regulation by Hox genes.** (A) *Ama* mRNA expression (green; lower panel monochrome) in *Dfd<sup>16</sup>,Scr<sup>4</sup>* mutant background counterstained with Engrailed (magenta). Compared to wild type expression (see middle panel in Fig 4D) *Ama* is upregulated in the *Scr*-expressing domain and downregulated in the *Dfd*-expressing domain (both marked with yellow box in lower panel) at early stage 11. (B) Quantification of the pixel intensities of



*Ama*-mRNA *in situ* hybridization in the *Scr*- or *Dfd*-expression domain of wild type and different Hox mutants (see Fig 4D–4H). Signals were normalized to the pixel intensity of *Ama*-expression in segment T3 of the corresponding embryo. Loss of *Scr* leads to an increase of *Ama*-expression, also in the *Dfd/Scr* double mutation. This might explain the reduced transformation rate of NB6-4max compared to *Dfd* single mutants (see Fig 3D and 3F). Loss of *Dfd* alone or in combination with *Scr*, *lab* or *Antp* leads to a strong reduction of *Ama* expression in the *Dfd*-expression domain. The y-axis shows the deviation of the pixel intensity in percentage from the wild type pixel intensity. (C) *Ama*-mRNA expression upon ectopic expression of *Antp*, *Scr* or *Dfd* using the *scaGal4* line. Only *Dfd* can strongly upregulate *Ama*-expression in ectopic areas (right panel). (D) Antibody staining for *Nrt* (green) and *Ama* (red, along with *pH3*, which is only in mitotic cells in the nucleus) at stage 10 shows that neuroectodermal cells (*ne*) and neuroblasts (NBs, *Mira* positive, blue) express both proteins. (E) In *Dfd*<sup>16</sup>/*Antp*<sup>7</sup> double mutants *Ama* protein is severely reduced. (F) Expression and localization of *Abl* (red, or monochrome in the lower panel) in wild type (left panel), *lab*<sup>1</sup>/*Dfd*<sup>12</sup> double mutants (middle panel) or *Abl*<sup>1</sup>/*Ama*<sup>R1</sup> double mutants (right panel). In wild type NBs *Abl* localizes to the cytoplasm with cortical enhancement. This localization is lost in both double mutant backgrounds. NB6-4max and labial glial precursors are marked with yellow arrow heads, neuronal precursor with white arrow heads. (G) Transheterozygous *Dfd*<sup>16</sup> mutants show a transformation of NB6-4max in 8% of all hemisegments. Scale bar is 10 μm. (TIF)

**S7 Fig. Overproliferation phenotypes in various mutant situations of the *Ama-Nrt-Abl* pathway, *lab,Dfd* double mutants or ectopic expression of constitutive-active *yki*<sup>S168A</sup>.** (A,B) In *Abl*<sup>1</sup>,*Ama*<sup>R1</sup>/*Abl*<sup>Δ</sup> (A) or *Abl*<sup>1</sup>,*Nrt*<sup>M54</sup>/*Abl*<sup>Δ</sup> (B) transheterozygous mutants cells with big nuclei (white arrow heads) can be observed. (C) Statistical analysis of the nuclear size of *Eg*-positive gnathal NBs in wild type (grey, n = 12 NBs) and *Abl*<sup>1</sup>,*Ama*<sup>R1</sup>/*Abl*<sup>Δ</sup> mutants (red, n = 23). The size difference is statistically highly significant increased in the mutant (t-test analysis, p<0,001). (D-I) Loss-of-function of *Abl*<sup>Δ</sup> (D), *Abl*<sup>1</sup>,*Nrt*<sup>M54</sup> (E), *Abl*<sup>1</sup>,*Ama*<sup>R1</sup> (F), *lab*<sup>1</sup>,*Dfd*<sup>12</sup> (G), *Nrt*<sup>1</sup> (H) or ectopic expression of constitutive-active *yki*<sup>S168A</sup> using the *scabrous*-Gal4 line (*scaGal4XUAS-yki*<sup>S168A</sup>; I) leads to massive overproliferation in the embryonic nervous system. (J) Triple mutation for *yki*<sup>B5</sup> and *lab*<sup>1</sup>,*Dfd*<sup>12</sup> shows a decrease in the transformation rate from 100% in the double mutants for *lab*<sup>1</sup>,*Dfd*<sup>12</sup> to 66% in the triple mutants. Thus, the loss of *yki* rescues the double mutant phenotype in 34% of all hemisegments. Scale bar is 10 μm. (TIF)

**S8 Fig. Influence of Hox genes on gnathal NB7-3 lineages and the formation of an ectopic mandibular NB6-4.** (A–C) Expression of Hox genes in NB7-3 in the gnathal segments in WT. (A) *Dfd* (red) is expressed in the mandibular NB7-3 and *Scr* (blue) in the maxillary NB7-3. (B) Proboscipedia (magenta) is only expressed in the mandibular NB7-3 lineage. (C) The labial NB7-3 expresses *Antp* (magenta), like the thoracic lineages. (D) At st16 the mandibular NB7-3 lineage in *Dfd*<sup>16</sup>/*Dfd*<sup>11</sup> transheterozygous mutants is not reduced to 2 cells like in WT. Instead, 5 to 6 cells survive until the end of embryogenesis (right and left panels of smaller pictures show magnifications of the mandibular NB7-3 clusters in different single layers to indicate all NB7-3 *Eg* (green) and *En* (red) positive cells). (E) In *Scr*<sup>11</sup> mutants the maxillary NB7-3 lineage is not reduced to the wild type number of 3 cells, instead, up to 8 *Eg* (green) and *En* (red) cells can be observed, shown in magnified single layers on the right side. (F) Formation of a mandibular NB6-4 lineage in 10% of *Dfd*<sup>16</sup> mutant hemisegments. NB6-4 glia cells are identified with co-expression of *Eg* (green) and *Repo* (magenta) in a possible position of an ectopically formed NB6-4 lineage. Scale bar is 10 μm. (TIF)

## Acknowledgments

We would like to thank I. Lohmann, F. Hirth, H. Reichert for helpful discussions and Olav Vef for help with fly genetics. We are very grateful to the following people for flies and antibodies: W. McGinnis, I. Silman, E. Giniger, F. Hirth, H. Reichert, T. Kaufman, E. Liebl, C. Doe, L. Fasano, J. Knoblich, K. Irvine, T. Halter, A. Nose, J. Ng, A. Percival-Smith, U. Waldorf, J. Reinitz, J. Jiang, J. Skeath, M. Odenwald, B. Altenhein, K. Wharton, T. von Ohlen, the Bloomington *Drosophila* Stock Center and the Developmental Studies Hybridoma Bank.

## Author Contributions

Conceived and designed the experiments: CB HB GMT. Performed the experiments: HB SR. Analyzed the data: HB CB GMT. Wrote the paper: HB CB GMT.

## References

1. Technau GM, Berger C, Urbach R. Generation of cell diversity and segmental pattern in the embryonic central nervous system of *Drosophila*. *Dev Dyn*. 2006; 235:861–869. PMID: [16222713](#)
2. Doe CQ. Molecular markers for identified neuroblasts and ganglion mother cells in the *Drosophila* central nervous system. *Development*. 1992; 116:855–863. PMID: [1295739](#)
3. Broadus J, Skeath JB, Spana EP, Bossing T, Technau G, Doe CQ. New neuroblast markers and the origin of the aCC/pCC neurons in the *Drosophila* central nervous system. *Mech Dev*. 1995; 53:393–402. PMID: [8645605](#)
4. Bossing T, Udolph G, Doe CQ, Technau GM. The embryonic central nervous system lineages of *Drosophila melanogaster*. I. Neuroblast lineages derived from the ventral half of the neuroectoderm. *Dev Biol*. 1996; 179:41–64. PMID: [8873753](#)
5. Schmid A, Chiba A, Doe CQ. Clonal analysis of *Drosophila* embryonic neuroblasts: neural cell types, axon projections and muscle targets. *Development*. 1999; 126:4653–4689. PMID: [10518486](#)
6. Schmidt H, Rickert C, Bossing T, Vef O, Urban J, Technau GM. The embryonic central nervous system lineages of *Drosophila melanogaster*. II. Neuroblast lineages derived from the dorsal part of the neuroectoderm. *Dev Biol*. 1997; 189:186–204. PMID: [9299113](#)
7. Berger C, Pallavi SK, Prasad M, Shashidhara LS, Technau GM. A critical role for *cyclin E* in cell fate determination in the central nervous system of *Drosophila melanogaster*. *Nat Cell Biol*. 2005; 7:56–62. PMID: [15580266](#)
8. Prokop A, Technau GM. Early tagma-specific commitment of *Drosophila* CNS progenitor NB1-1. *Development*. 1994; 120:2567–2578. PMID: [7956832](#)
9. Prokop A, Bray S, Harrison E, Technau GM. Homeotic regulation of segment-specific differences in neuroblast numbers and proliferation in the *Drosophila* central nervous system. *Mech Dev*. 1998; 74:99–110. PMID: [9651493](#)
10. Lewis EB. A gene complex controlling segmentation in *Drosophila*. *Nature*. 1978; 276:565–570. PMID: [103000](#)
11. Bachiller D, Macías A, Duboule D, Morata G. Conservation of a functional hierarchy between mammalian and insect Hox/HOM genes. *EMBO J*. 1994; 13:1930–1941. PMID: [7909514](#)
12. Duboule D, Morata G. Colinearity and functional hierarchy among genes of the homeotic complexes. *Trends Genet*. 1994; 10:358–364. PMID: [7985240](#)
13. Birkholz O, Vef O, Rogulja-Ortmann A, Berger C, Technau GM. Abdominal-B and caudal inhibit the formation of specific neuroblasts in the *Drosophila* tail region. *Development*. 2013; 140:3552–3564. doi: [10.1242/dev.096099](#) PMID: [23903193](#)
14. Birkholz O, Rickert C, Berger C, Urbach R, Technau GM. Neuroblast pattern and identity in the *Drosophila* tail region and role of doublesex in the survival of sex-specific precursors. *Development*. 2013; 140:1830–1842. doi: [10.1242/dev.090043](#) PMID: [23533181](#)
15. Schmidt-Ott U, Technau GM. Expression of *en* and *wg* in the embryonic head and brain of *Drosophila* indicates a refolded band of seven segment remnants. *Development*. 1992; 116:111–125. PMID: [1483381](#)
16. Schmidt-Ott U, González-Gaitán M, Jäckle H, Technau GM. Number, identity, and sequence of the *Drosophila* head segments as revealed by neural elements and their deletion patterns in mutants. *Proc Natl Acad Sci U S A*. 1994; 91:8363–8367. PMID: [7915837](#)

17. Urbach R, Technau GM. Molecular markers for identified neuroblasts in the developing brain of *Drosophila*. *Development*. 2003; 130:3621–3637. PMID: [12835380](#)
18. Urbach R, Technau GM. Segment polarity and DV patterning gene expression reveals segmental organization of the *Drosophila* brain. *Development*. 2003; 130:3607–3620. PMID: [12835379](#)
19. Urbach R, Technau GM. Neuroblast formation and patterning during early brain development in *Drosophila*. *Bioessays*. 2004; 26:739–751. PMID: [15221856](#)
20. Dittrich R, Bossing T, Gould AP, Technau GM, Urban J. The differentiation of the serotonergic neurons in the *Drosophila* ventral nerve cord depends on the combined function of the zinc finger proteins Eagle and Hucklebein. *Development*. 1997; 124:2515–2525. PMID: [9216994](#)
21. Higashijima S, Shishido E, Matsuzaki M, Saigo K. *eagle*, a member of the steroid receptor gene superfamily, is expressed in a subset of neuroblasts and regulates the fate of their putative progeny in the *Drosophila* CNS. *Development*. 1996; 122:527–536. PMID: [8625804](#)
22. Fremion F, Darboux I, Diano M, Hipeau-Jacquotte R, Seeger MA, Piovant M. Amalgam is a ligand for the transmembrane receptor *neurotactin* and is required for neurotactin-mediated cell adhesion and axon fasciculation in *Drosophila*. *EMBO J*. 2000; 19:4463–4472. PMID: [10970840](#)
23. Liebl EC, Rowe RG, Forsthoefel DJ et al. Interactions between the secreted protein Amalgam, its transmembrane receptor Neurotactin and the Abelson tyrosine kinase affect axon pathfinding. *Development*. 2003; 130:3217–3226. PMID: [12783792](#)
24. Seeger MA, Haffley L, Kaufman TC. Characterization of *amalgam*: a member of the immunoglobulin superfamily from *Drosophila*. *Cell*. 1988; 55:589–600. PMID: [3141062](#)
25. Zeev-Ben-Mordehai T, Paz A, Peleg Y et al. Amalgam, an axon guidance *Drosophila* adhesion protein belonging to the immunoglobulin superfamily: over-expression, purification and biophysical characterization. *Protein Expr Purif*. 2009; 63:147–157. doi: [10.1016/j.pep.2008.09.019](#) PMID: [18938249](#)
26. Kannan R, Berger C, Myneni S, Technau GM, Shashidhara LS. Abdominal-A mediated repression of Cyclin E expression during cell-fate specification in the *Drosophila* central nervous system. *Mech Dev*. 2010; 127:137–145. doi: [10.1016/j.mod.2009.09.008](#) PMID: [19799999](#)
27. Bier E, Vaessin H, Younger-Shepherd S, Jan LY, Jan YN. *deadpan*, an essential pan-neural gene in *Drosophila*, encodes a helix-loop-helix protein similar to the hairy gene product. *Genes Dev*. 1992; 6:2137–2151. PMID: [1427077](#)
28. Dambly-Chaudière C, Jamet E, Burri M et al. The paired box gene *pox neuro*: a determinant of poly-innervated sense organs in *Drosophila*. *Cell*. 1992; 69:159–172. PMID: [1348214](#)
29. Dormand EL, Brand AH. Runt determines cell fates in the *Drosophila* embryonic CNS. *Development*. 1998; 125:1659–1667. PMID: [9521904](#)
30. Lundell MJ, Hirsh J. *eagle* is required for the specification of serotonin neurons and other neuroblast 7–3 progeny in the *Drosophila* CNS. *Development*. 1998; 125:463–472. PMID: [9425141](#)
31. Desphande N, Dittrich R, Technau G, Urban J. Successive specification of *Drosophila* NB6-4 and NB7-3 depends on interaction of the segment polarity genes *wingless*, *gooseberry* and *naked cuticle*. *Development*. 2001; 128:3253–3261. PMID: [11546742](#)
32. Skeath JB, Zhang Y, Holmgren R, Carroll SB, Doe CQ. Specification of neuroblast identity in the *Drosophila* embryonic central nervous system by *gooseberry-distal*. *Nature*. 1995; 376:427–430. PMID: [7630418](#)
33. Doe CQ, Spana EP. A collection of cortical crescents: asymmetric protein localization in CNS precursor cells. *Neuron*. 1995; 15:991–995. PMID: [7576667](#)
34. Kammermeier L, Leemans R, Hirth F et al. Differential expression and function of the *Drosophila* Pax6 genes *eyeless* and *twin of eyeless* in embryonic central nervous system development. *Mech Dev*. 2001; 103:71–78. PMID: [11335113](#)
35. Rogulja-Ortmann A, Luer K, Seibert J, Rickert C, Technau GM. Programmed cell death in the embryonic central nervous system of *Drosophila melanogaster*. *Development*. 2007; 134:105–116. PMID: [17164416](#)
36. Rogulja-Ortmann A, Renner S, Technau GM. Antagonistic roles for Ultrabithorax and Antennapedia in regulating segment-specific apoptosis of differentiated motoneurons in the *Drosophila* embryonic central nervous system. *Development*. 2008; 135:3435–3445. doi: [10.1242/dev.023986](#) PMID: [18799545](#)
37. Halter DA, Urban J, Rickert C et al. The homeobox gene *reversed-polarity* is required for the differentiation and maintenance of glia function in the embryonic nervous system of *Drosophila melanogaster*. *Development*. 1995; 121:317–332. PMID: [7768175](#)
38. Berger C, Kannan R, Myneni S, Renner S, Shashidhara LS, Technau GM. Cell cycle independent role of Cyclin E during neural cell fate specification in *Drosophila* is mediated by its regulation of Prospero function. *Dev Biol*. 2010; 337:415–424. doi: [10.1016/j.ydbio.2009.11.012](#) PMID: [19914234](#)

39. Bernardoni R, Kammerer M, Vonesch JL, Giangrande A. Gliogenesis depends on *glide/gcm* through asymmetric division of neuroglioblasts. *Dev Biol.* 1999; 216:265–275. PMID: [10588877](#)
40. Freeman MR, Doe CQ. Asymmetric Prospero localization is required to generate mixed neuronal/glia lineages in the *Drosophila* CNS. *Development.* 2001; 128:4103–4112. PMID: [11641232](#)
41. Crews ST, Thomas JB, Goodman CS. The *Drosophila single-minded* gene encodes a nuclear protein with sequence similarity to the per gene product. *Cell.* 1988; 52:143–151. PMID: [3345560](#)
42. Wheeler SR, Kearney JB, Guardiola AR, Crews ST. Single-cell mapping of neural and glial gene expression in the developing *Drosophila* CNS midline cells. *Dev Biol.* 2006; 294:509–524. PMID: [16631157](#)
43. Buenzow DE, Holmgren R. Expression of the *Drosophila gooseberry* locus defines a subset of neuroblast lineages in the central nervous system. *Dev Biol.* 1995; 170:338–349. PMID: [7649367](#)
44. De Graeve F, Jagla T, Daponte JP et al. The *ladybird* homeobox genes are essential for the specification of a subpopulation of neural cells. *Dev Biol.* 2004; 270:122–134. PMID: [15136145](#)
45. Weiss JB, Von Ohlen T, Mellerick DM, Dressler G, Doe CQ, Scott MP. Dorsoventral patterning in the *Drosophila* central nervous system: the *intermediate neuroblasts defective* homeobox gene specifies intermediate column identity. *Genes Dev.* 1998; 12:3591–3602. PMID: [9832510](#)
46. Berger C, Pallavi SK, Prasad M, Shashidhara LS, Technau GM. Cyclin E acts under the control of Hox genes as a cell fate determinant in the developing central nervous system. *Cell Cycle.* 2005; 4: 422–425. PMID: [15684605](#)
47. Mahaffey JW, Diederich RJ, Kaufman TC. Novel patterns of homeotic protein accumulation in the head of the *Drosophila* embryo. *Development.* 1989; 105:167–174. PMID: [2572411](#)
48. Martinez-Arias A, Ingham PW, Scott MP, Akam ME. The spatial and temporal deployment of *Dfd* and *Scr* transcripts throughout development of *Drosophila*. *Development.* 1987; 100:673–683. PMID: [2450726](#)
49. Diederich RJ, Pattatucci AM, Kaufman TC. Developmental and evolutionary implications of *labial*, *Deformed* and *engrailed* expression in the *Drosophila* head. *Development.* 1991; 113:273–281. PMID: [1684933](#)
50. Hirth F, Hartmann B, Reichert H. Homeotic gene action in embryonic brain development of *Drosophila*. *Development.* 1998; 125:1579–1589. PMID: [9521896](#)
51. Hueber SD, Bezdan D, Henz SR, Blank M, Wu H, Lohmann I. Comparative analysis of Hox downstream genes in *Drosophila*. *Development.* 2007; 134:381–392. PMID: [17166915](#)
52. Leemans R, Loop T, Egger B et al. Identification of candidate downstream genes for the homeodomain transcription factor Labial in *Drosophila* through oligonucleotide-array transcript imaging. *Genome Biol.* 2001; 2:RESEARCH0015. PMID: [11387036](#)
53. Datta RR, Weasner BP, Kumar JP. A dissection of the *teashirt* and *tiptop* genes reveals a novel mechanism for regulating transcription factor activity. *Dev Biol.* 2011; 360:391–402. doi: [10.1016/j.ydbio.2011.09.030](#) PMID: [22019301](#)
54. de Zulueta P, Alexandre E, Jacq B, Kerridge S. Homeotic complex and *teashirt* genes co-operate to establish trunk segmental identities in *Drosophila*. *Development.* 1994; 120:2287–2296. PMID: [7925029](#)
55. Mahaffey JW, Griswold CM, Cao QM. The *Drosophila* genes *disconnected* and *disco-related* are redundant with respect to larval head development and accumulation of mRNAs from deformed target genes. *Genetics.* 2001; 157:225–236. PMID: [11139504](#)
56. Röder L, Vola C, Kerridge S. The role of the *teashirt* gene in trunk segmental identity in *Drosophila*. *Development.* 1992; 115:1017–1033. PMID: [1360402](#)
57. Steller H, Fischbach KF, Rubin GM. Disconnected: a locus required for neuronal pathway formation in the visual system of *Drosophila*. *Cell.* 1987; 50:1139–1153. PMID: [3113740](#)
58. Ebner A, Cabernard C, Affolter M, Merabet S. Recognition of distinct target sites by a unique Labial/Extradenticle/Homothorax complex. *Development.* 2005; 132:1591–1600. PMID: [15753213](#)
59. Joshi R, Sun L, Mann R. Dissecting the functional specificities of two Hox proteins. *Genes Dev.* 2010; 24:1533–1545. doi: [10.1101/gad.1936910](#) PMID: [20634319](#)
60. Affolter M, Percival-Smith A, Müller M, Leupin W, Gehring WJ. DNA binding properties of the purified Antennapedia homeodomain. *Proc Natl Acad Sci U S A.* 1990; 87:4093–4097. PMID: [1971945](#)
61. Joshi R, Passner JM, Rohs R et al. Functional specificity of a Hox protein mediated by the recognition of minor groove structure. *Cell.* 2007; 131:530–543. PMID: [17981120](#)
62. Song JK, Kannan R, Merdes G, Singh J, Mlodzik M, Giniger E. Disabled is a bona fide component of the Abl signaling network. *Development.* 2010; 137:3719–3727. doi: [10.1242/dev.050948](#) PMID: [20940230](#)

63. Gertler FB, Doctor JS, Hoffmann FM. Genetic suppression of mutations in the *Drosophila abl* proto-oncogene homolog. *Science*. 1990; 248:857–860. PMID: [2188361](#)
64. Liebl EC, Forsthoefel DJ, Franco LS et al. Dosage-sensitive, reciprocal genetic interactions between the Abl tyrosine kinase and the putative GEF *trio* reveal trio's role in axon pathfinding. *Neuron*. 2000; 26:107–118. PMID: [10798396](#)
65. Barzik M, Kotova TI, Higgs HN et al. Ena/VASP proteins enhance actin polymerization in the presence of barbed end capping proteins. *J Biol Chem*. 2005; 280:28653–28662. PMID: [15939738](#)
66. Bear JE, Svitkina TM, Krause M et al. Antagonism between Ena/VASP proteins and actin filament capping regulates fibroblast motility. *Cell*. 2002; 109:509–521. PMID: [12086607](#)
67. Grevengoed EE, Fox DT, Gates J, Peifer M. Balancing different types of actin polymerization at distinct sites: roles for Abelson kinase and Enabled. *J Cell Biol*. 2003; 163:1267–1279. PMID: [14676307](#)
68. Smith JA, Liebl EC. Identification of the molecular lesions in alleles of the *Drosophila* Abelson tyrosine kinase. *Drosophila* Information Service. 2005; 88:20–22.
69. Grevengoed EE, Loureiro JJ, Jesse TL, Peifer M. Abelson kinase regulates epithelial morphogenesis in *Drosophila*. *J Cell Biol*. 2001; 155:1185–1198. PMID: [11756472](#)
70. Henkemeyer M, West SR, Gertler FB, Hoffmann FM. A novel tyrosine kinase-independent function of *Drosophila abl* correlates with proper subcellular localization. *Cell*. 1990; 63:949–960. PMID: [2175256](#)
71. Bennett RL, Hoffmann FM. Increased levels of the *Drosophila* Abelson tyrosine kinase in nerves and muscles: subcellular localization and mutant phenotypes imply a role in cell-cell interactions. *Development*. 1992; 116:953–966. PMID: [1295746](#)
72. Stevens TL, Rogers EM, Koontz LM et al. Using *bcr-abl* to examine mechanisms by which *abl* kinase regulates morphogenesis in *Drosophila*. *Mol Biol Cell*. 2008; 19:378–393. PMID: [17959833](#)
73. Levy D, Adamovich Y, Reuven N, Shaul Y. Yap1 phosphorylation by c-Abl is a critical step in selective activation of proapoptotic genes in response to DNA damage. *Mol Cell*. 2008; 29:350–361. doi: [10.1016/j.molcel.2007.12.022](#) PMID: [18280240](#)
74. Liu W, Wu J, Xiao L et al. Regulation of neuronal cell death by c-Abl-Hippo/MST2 signaling pathway. *PLoS One*. 2012; 7:e36562. doi: [10.1371/journal.pone.0036562](#) PMID: [22590567](#)
75. Halder G, Johnson RL. Hippo signaling: growth control and beyond. *Development*. 2011; 138:9–22. doi: [10.1242/dev.045500](#) PMID: [21138973](#)
76. Harvey K, Tapon N. The Salvador-Warts-Hippo pathway—an emerging tumour-suppressor network. *Nat Rev Cancer*. 2007; 7:182–191. PMID: [17318211](#)
77. Pan D. The hippo signaling pathway in development and cancer. *Dev Cell*. 2010; 19:491–505. doi: [10.1016/j.devcel.2010.09.011](#) PMID: [20951342](#)
78. Pantalacci S, Tapon N, Leopold P. The Salvador partner Hippo promotes apoptosis and cell-cycle exit in *Drosophila*. *Nat Cell Biol*. 2003; 5:921–927. PMID: [14502295](#)
79. Aerne BL, Gailite I, Sims D, Tapon N. Hippo Stabilises Its Adaptor Salvador by Antagonising the HECT Ubiquitin Ligase Herc4. *PLoS One*. 2015; 10:e0131113. doi: [10.1371/journal.pone.0131113](#) PMID: [26125558](#)
80. Huang J, Wu S, Barrera J, Matthews K, Pan D. The Hippo Signaling Pathway Coordinately Regulates Cell Proliferation and Apoptosis by Inactivating Yorkie, the *Drosophila* Homolog of YAP. *Cell*. 2005; 122:421–434. PMID: [16096061](#)
81. Zhao B, Tumaneng K, Guan KL. The Hippo pathway in organ size control, tissue regeneration and stem cell self-renewal. *Nat Cell Biol*. 2011; 13:877–883. doi: [10.1038/ncb2303](#) PMID: [21808241](#)
82. Oh H, Irvine KD. In vivo regulation of Yorkie phosphorylation and localization. *Development*. 2008; 135:1081–1088. doi: [10.1242/dev.015255](#) PMID: [18256197](#)
83. Bhat KM. Segment polarity genes in neuroblast formation and identity specification during *Drosophila* neurogenesis. *Bioessays*. 1999; 21:472–485. PMID: [10402954](#)
84. Skeath JB. At the nexus between pattern formation and cell-type specification: the generation of individual neuroblast fates in the *Drosophila* embryonic central nervous system. *Bioessays*. 1999; 21:922–931. PMID: [10517865](#)
85. Udolph G, Prokop A, Bossing T, Technau GM. A common precursor for glia and neurons in the embryonic CNS of *Drosophila* gives rise to segment-specific lineage variants. *Development*. 1993; 118:765–775. PMID: [8076516](#)
86. Technau GM, Rogulja-Ortmann A, Berger C, Birkholz O, Rickert C. Composition of a Neuromere and Its Segmental Diversification under the Control of Hox Genes in the Embryonic CNS of *Drosophila*. *J Neurogenet*. 2014:1–10.
87. Morata G. Homeotic genes of *Drosophila*. *Curr Opin Genet Dev*. 1993; 3:606–614. PMID: [7902147](#)

88. Miller DF, Rogers BT, Kalkbrenner A, Hamilton B, Holtzman SL, Kaufman T. Cross-regulation of Hox genes in the *Drosophila melanogaster* embryo. *Mech Dev*. 2001; 102:3–16. PMID: [11287177](#)
89. González-Reyes A, Macías A, Morata G. Autocatalysis and phenotypic expression of *Drosophila* homeotic gene *Deformed*: its dependence on polarity and homeotic gene function. *Development*. 1992; 116:1059–1068. PMID: [1363540](#)
90. Papagiannouli F, Schardt L, Grajcarek J, Ha N, Lohmann I. The Hox gene *Abd-B* controls stem cell niche function in the *Drosophila* testis. *Dev Cell*. 2014; 28:189–202. doi: [10.1016/j.devcel.2013.12.016](#) PMID: [24480643](#)
91. Bashaw GJ, Kidd T, Murray D, Pawson T, Goodman CS. Repulsive axon guidance: Abelson and Enabled play opposing roles downstream of the *roundabout* receptor. *Cell*. 2000; 101:703–715. PMID: [10892742](#)
92. Wills Z, Marr L, Zinn K, Goodman CS, Van Vactor D. Profilin and the Abl tyrosine kinase are required for motor axon outgrowth in the *Drosophila* embryo. *Neuron*. 1999; 22:291–299. PMID: [10069335](#)
93. Lanier LM, Gertler FB. From Abl to actin: Abl tyrosine kinase and associated proteins in growth cone motility. *Curr Opin Neurobiol*. 2000; 10:80–87. PMID: [10679439](#)
94. Brumby A, Secombe J, Horsfield J et al. A Genetic Screen for Dominant Modifiers of a cyclin E Hypomorphic Mutation Identifies Novel Regulators of S-Phase Entry in *Drosophila*. *Genetics*. 2004; 168:227–251. PMID: [15454540](#)
95. Mo JS, Meng Z, Kim YC et al. Cellular energy stress induces AMPK-mediated regulation of YAP and the Hippo pathway. *Nat Cell Biol*. 2015; 17:500–510. doi: [10.1038/ncb3111](#) PMID: [25751140](#)
96. Gailite I, Aerne BL, Tapon N. Differential control of Yorkie activity by LKB1/AMPK and the Hippo/Warts cascade in the central nervous system. *Proc Natl Acad Sci U S A*. 2015
97. Andrew DJ, Horner MA, Pettitt MG, Smolik SM, Scott MP. Setting limits on homeotic gene function: restraint of Sex combs reduced activity by *teashirt* and other homeotic genes. *EMBO J*. 1994; 13:1132–1144. PMID: [7907545](#)
98. Fasano L, Röder L, Coré N et al. The gene *teashirt* is required for the development of *Drosophila* embryonic trunk segments and encodes a protein with widely spaced zinc finger motifs. *Cell*. 1991; 64:63–79. PMID: [1846092](#)
99. Laugier E, Yang Z, Fasano L, Kerridge S, Vola C. A critical role of *teashirt* for patterning the ventral epidermis is masked by ectopic expression of *tiptop*, a paralog of *teashirt* in *Drosophila*. *Dev Biol*. 2005; 283:446–458. PMID: [15936749](#)
100. Wharton KA, Cook JM, Torres-Schumann S, de Castro K, Borod E, Phillips DA. Genetic analysis of the *bone morphogenetic protein*-related gene, *gbb*, identifies multiple requirements during *Drosophila* development. *Genetics*. 1999; 152:629–640. PMID: [10353905](#)
101. Umemiya T, Takeichi M, Nose A. M-spondin, a novel ECM protein highly homologous to vertebrate F-spondin, is localized at the muscle attachment sites in the *Drosophila* embryo. *Dev Biol*. 1997; 186:165–176. PMID: [9205137](#)
102. Baker NE. Molecular cloning of sequences from *wingless*, a segment polarity gene in *Drosophila*: the spatial distribution of a transcript in embryos. *EMBO J*. 1987; 6:1765–1773. PMID: [16453776](#)
103. Kurata S, Go MJ, Artavanis-Tsakonas S, Gehring WJ. Notch signaling and the determination of appendage identity. *Proc Natl Acad Sci U S A*. 2000; 97:2117–2122. PMID: [10681430](#)
104. Li X, Murre C, McGinnis W. Activity regulation of a Hox protein and a role for the homeodomain in inhibiting transcriptional activation. *EMBO J*. 1999; 18:198–211. PMID: [9878063](#)
105. Percival-Smith A, Teft WA, Barta JL. Tarsus determination in *Drosophila melanogaster*. *Genome*. 2005; 48:712–721. PMID: [16094438](#)
106. Karcavich R, Doe CQ. *Drosophila* neuroblast 7–3 cell lineage: a model system for studying programmed cell death, Notch/Numb signaling, and sequential specification of ganglion mother cell identity. *J Comp Neurol*. 2005; 481:240–251. PMID: [15593370](#)
107. von Hilchen CM, Bustos AE, Giangrande A, Technau GM, Altenhein B. Predetermined embryonic glial cells form the distinct glial sheaths of the *Drosophila* peripheral nervous system. *Development*. 2013; 140:3657–3668. doi: [10.1242/dev.093245](#) PMID: [23903191](#)
108. Jack T, McGinnis W. Establishment of the *Deformed* expression stripe requires the combinatorial action of coordinate, gap and pair-rule proteins. *EMBO J*. 1990; 9:1187–1198. PMID: [2323337](#)
109. Randazzo FM, Cribbs DL, Kaufman TC. Rescue and regulation of *proboscipedia*: a homeotic gene of the Antennapedia Complex. *Development*. 1991; 113:257–271. PMID: [1684932](#)
110. Kambadur R, Koizumi K, Stivers C, Nagle J, Poole SJ, Odenwald WF. Regulation of POU genes by *castor* and *hunchback* establishes layered compartments in the *Drosophila* CNS. *Genes Dev*. 1998; 12:246–260. PMID: [9436984](#)

111. Zhang Y, Ungar A, Fresquez C, Holmgren R. Ectopic expression of either the *Drosophila* *gooseberry-distal* or *proximal* gene causes alterations of cell fate in the epidermis and central nervous system. *Development*. 1994; 120:1151–1161. PMID: [8026326](#)
112. Kosman D, Small S, Reinitz J. Rapid preparation of a panel of polyclonal antibodies to *Drosophila* segmentation proteins. *Dev Genes Evol*. 1998; 208:290–294. PMID: [9683745](#)
113. Von Ohlen TL, Moses C. Identification of Ind transcription activation and repression domains required for dorsoventral patterning of the CNS. *Mech Dev*. 2009; 126:552–562. doi: [10.1016/j.mod.2009.03.008](#) PMID: [19348939](#)
114. Yue T, Tian A, Jiang J. The cell adhesion molecule *echinoid* functions as a tumor suppressor and upstream regulator of the Hippo signaling pathway. *Dev Cell*. 2012; 22:255–267. doi: [10.1016/j.devcel.2011.12.011](#) PMID: [22280890](#)